New Journal of Physics
The open access journal at the forefront of physics

Deutsche Physikalische Gesellschaft DPG
IOP Institute of Physics

Published in partnership with: Deutsche Physikalische Gesellschaft and the Institute of Physics

OPEN ACCESS

RECEIVED
10 September 2014

ACCEPTED FOR PUBLICATION
3 December 2014

PUBLISHED
15 January 2015

PAPER

Computation of rare transitions in the barotropic quasi-geostrophic equations

Jason Laurie[1] **and Freddy Bouchet**[2]

[1] Department of Physics of Complex Systems, Weizmann Institute of Science, 234 Herzl Street, Rehovot, 76100, Israel
[2] Laboratoire de Physique, ENS de Lyon, 46, Allée d'Italie, F69007, Lyon, France

E-mail: jason.laurie@weizmann.ac.il **and** freddy.bouchet@ens-lyon.fr

Keywords: rare transitions, bistability, minimum action method, quasi-geostrophic dynamics

Abstract

We investigate the theoretical and numerical computation of rare transitions in simple geophysical turbulent models. We consider the barotropic quasi-geostrophic and two-dimensional Navier–Stokes equations in regimes where bistability between two coexisting large-scale attractors exist. By means of large deviations and instanton theory with the use of an Onsager–Machlup path integral formalism for the transition probability, we show how one can directly compute the most probable transition path between two coexisting attractors analytically in an equilibrium (Langevin) framework and numerically otherwise. We adapt a class of numerical optimization algorithms known as minimum action methods to simple geophysical turbulent models. We show that by numerically minimizing an appropriate action functional in a large deviation limit, one can predict the most likely transition path for a rare transition between two states. By considering examples where theoretical predictions can be made, we show that the minimum action method successfully predicts the most likely transition path. Finally, we discuss the application and extension of such numerical optimization schemes to the computation of rare transitions observed in direct numerical simulations and experiments and to other, more complex, turbulent systems.

1. Introduction

Many turbulent flows related to climate dynamics undergo sporadic random transitions [1]: after long periods of apparent statistical stationarity close to one of the dynamical attractors, they spontaneously switch to another dynamical attractor. In recent years, there has been increasing evidence that indicates that the ocean circulation has multiple attractors [2] corresponding to different regimes of thermohaline circulation, driven by salinity and temperature differences between the poles and the equator. The transition between such attractors may be related to Dansgaard–Oeschger events [2, 3]. Transitions between two attractors (bistability) is also observed at large scales of ocean currents, for instance the Kuroshio [4, 5]. The importance of possible bistability and abrupt transitions has been emphasized many times, including for the planetary atmosphere [6–11], where planetary jets may have a huge impact on abrupt climate change [8, 12, 13].

Random transitions in turbulent flows are also extremely prevalent in astrophysics and geophysics as well as in laboratories and industrial applications. For instance, the Earth's magnetic field reversal is a transition between two turbulent attractors just as in magneto-hydrodynamics experiments [14]. Bistability is also observed in two-dimensional turbulence simulations and experiments [15–17] and in Rayleigh–Bénard convection cells [18–21], and dozens of other three-dimensional fluid flows show this kind of behavior. (See, for instance, [22] and [17] for more references.)

Stochastic resonance [23, 24] has been advocated as a possible mechanism for the abrupt transitions between glacial and inter-glacial periods, and in relation to bistability of climate dynamics and time-varying forces (i.e., the Milankovitch cycles [25]). The hypothesis of stochastic resonance is debated [23, 26] because of the disparity between simple models of only a few degrees of freedom that are used conceptually [23, 24] and more complex

models. Stochastic resonance, however, remains a very interesting possibility. To address such issues one should study the attractors and the dynamics of the rare transition between attractors in a hierarchy of models from the simplest to more complex ones used by the climate community. For these complex climate models, which genuinely reproduce the turbulent nature of the Earth's atmosphere and ocean dynamics, such a task is currently inconceivable and seems unreachable in the foreseeable future using direct numerical simulations. The reasons are the rarity of the transitions and the computational complexity of these models. The main aim of this paper is to make a step in the direction of this challenge by studying bistability and the associated transitions in turbulent dynamics using tools that will allow one to compute transitions in more complex systems in the near future.

These rare transitions are essential phenomena because they correspond to drastic changes in complex system behavior. Moreover, they cannot be studied using conventional tools. They contain dynamics occurring on multiple and extremely different timescales, usually with no spectral gap. This prevents the use of classical tools from dynamical system theory. The theoretical understanding of these transitions is an extremely difficult problem due to the complexity, the large number of degrees of freedom, and the non-equilibrium nature of many of these flows. Up to now, there have been an extremely limited number of theoretical results, where analysis has been limited to analogies with models of very few degrees of freedom [27] or to specific classes of systems that can be directly related to equilibrium Langevin dynamics [28]. For this reason, the use of non-equilibrium statistical mechanics to study these dynamics is necessary.

The main problem is in how to develop a general theory for these phenomena. When a complex turbulent flow switches at random from one subregion of the phase space to another, the first theoretical aim is to characterize and predict the observed attractors. This is already a nontrivial task because no picture, based on a potential landscape, is available. Indeed, this is especially tricky when the transition is not related to any symmetry breaking. An additional theoretical challenge is in being able to compute the transition rates between attractors. It is also often the case that most transition paths from one attractor to another concentrate close to a single unique path; therefore, a natural objective is to compute this most probable transition path. To achieve these goals, it is convenient to think about the framework of large deviation theory either to describe the stationary distribution of the system or to compute the transition probabilities of the stochastic process. In principle, we can argue that from a path integral representation of the transition probability [29] and the study of its semi-classical limit in an asymptotic expansion, with a well-chosen small parameter we can derive a large deviation rate function that would characterize the attractors and various other properties of the system. When this semi-classical approach is relevant, one expects a large deviation result, similar to that obtained through the Freidlin–Wentzell theory [30]. If this notion is correct, this would explain why these rare transitions share many analogies with phase transitions in statistical mechanics and stochastic dynamics with few degrees of freedom.

On the mathematical side, the study of sufficient hypotheses in order to rigorously prove such large deviation results is one of the main aspects of Freidlin–Wentzell theory [30]. However, we draw the attention of the reader to the fact that for infinite dimensional field equations, e.g., turbulence models, a large deviation result is far from obvious in the weak noise limit. It may be expected to be the case if, for instance, the degrees of freedom on the smallest scales can be proven to have a negligible effect on the dynamics, such that they are qualitatively similar to those of an effective finite dimensional system. For the turbulence model we present here, such a property is not obvious at all. Studying this issue in general is an extremely difficult task and goes beyond the scope of this paper. Similar questions have been addressed in the past in the context of the Allen–Cahn or the stochastic Ginzburg–Landau equations in relation to stochastic quantization [31, 32], with very appealing new results in larger dimensions [33, 34].

Therefore, with this in mind, we consider the simplest turbulent systems that exhibit random transitions between multiple coexisting attractors. The quasi-geostrophic model with stochastic forces is simple enough to be studied from first principles, in the framework of statistical mechanics and large deviation theory. Moreover, this model is relevant to describe some aspects of the largest scales of turbulent geophysical fluid dynamics. The model shares many analogies with the two-dimensional Euler and Navier–Stokes equation [35]. These systems include the one-layer quasi-geostrophic model and its subsidiary, the two-dimensional Navier–Stokes equations. For instance, in [17], the authors observed rare transitions between two quasi-stable large-scale flow configurations, namely a dual-band zonal jet and a vortex dipole for the stochastically forced two-dimensional Navier–Stokes equations in the limit of weak noise and dissipation. In geophysical fluid dynamics, zonal jets or zonal flows occur when the velocity field is aligned with latitude circles, and they depend only on the longitude coordinate y, i.e., $\mathbf{v} = U(y)\mathbf{e}_x$. Furthermore, multiple zonal jet configurations were observed as dynamical attractors in the quasi-geostrophic model for the same set of parameters [36]. These examples provide the necessary motivation to try to understand rare transitions between two attractors for geophysical fluid flows. The goal is to develop a theory that will be able to predict the most likely transition path between two attractors without having to resort to direct observations of rare events in nature, computationally expensive numerical simulations, or costly experimental setups.

To this end, we develop a non-equilibrium statistical mechanics description for the prediction of the most probable rare transitions between two coexisting attractors. By considering the transition probability of all the possible transition paths between the two states as a Feynman path integral, we apply a saddle-point approximation, in an appropriate limit characterizing the rarity of these transitions, in order to determine the path that yields the greatest contribution to the transition probability. We decompose the problem into two subclasses: equilibrium and non-equilibrium. Through an equilibrium hypothesis, we are able to make direct analytical predictions from the path integral formalism for the most probable transition path. In this case any transition away from an attractor will become rare in the limit of weak noise. Alternatively, the non-equilibrium problem is more complex. In many cases, we are obliged to resort to numerically computing the most probable rare transition through numerical optimization techniques. We outline an appropriate algorithm for use in turbulent models considered here and show that the numerical predictions agree with theoretical results when obtainable.

The layout of this manuscript is as follows: In section 2 we discuss the class of turbulence models (the barotropic quasi-geostrophic and two-dimensional Navier–Stokes equations) and detail the path integral formalism for the Freidlin and Wentzell (instanton) approach. In section 3, we provide an overview of recent theoretical results of these models in a purely equilibrium Langevin setup. In such cases, rare trajectories can be directly computed by considering relaxation (deterministic) trajectories of a corresponding dual dynamics. By considering a simple example where a first- and second-order phase transition occurs through bifurcation of a tri-critical point, we show that the predicted rare trajectories agree with new direct numerical simulations of the system for a transition between two zonal jets. Section 4 details a numerical optimization algorithm used to compute the most probable rare transition in the barotropic quasi-geostrophic and two-dimensional Navier–Stokes equations in both the equilibrium and non-equilibrium regimes. In section 5 we apply the numerical method from the previous section to several examples of rare transitions in geophysical flows where analytical predictions can be made. Moreover, we consider an important generalized example of bistability in geophysics: a non-equilibrium transition between two distinct zonal jets with topography. We show how the numerical optimization algorithm predicts a transition that remains in the set of zonal jet states, thus greatly simplifying the accompanying theory. Finally, we conclude in section 6 by discussing the relevance of the equilibrium and non-equilibrium setups, the advantages and disadvantages of the numerical procedure, and the possible extension of this method to more complex turbulent systems.

2. The barotropic quasi-geostrophic and two-dimensional Navier–Stokes equations

The most simple turbulent model relevant to bistability in geophysical fluid dynamics is arguably the stochastically forced one-layer barotropic quasi-geostrophic model inside a periodic domain of size $\mathcal{D} = [0, L_x) \times [0, L_y)$ with aspect ratio $\delta = L_x/L_y$:

$$\frac{\partial q}{\partial t} + \mathbf{v} \cdot \nabla q = -\alpha\omega - \nu(-\Delta)^n\omega + \sqrt{\sigma}\eta, \tag{1a}$$

$$\mathbf{v} = \mathbf{e}_z \times \nabla\psi, \qquad q = \omega + h(\mathbf{r}) = \Delta\psi + h(\mathbf{r}), \tag{1b}$$

where ω, q, $\mathbf{v}$, and ψ are the vorticity, the potential vorticity, the non-divergent velocity, and the streamfunction respectively.

The topography is defined through the function $h(\mathbf{r})$. If we set $h \equiv 0$, then the barotropic quasi-geostrophic equation (1) reduces to the two-dimensional Navier–Stokes equation with linear friction and hyperviscosity. We consider G to be the Green's function of the Laplacian operator ($G = \Delta^{-1}$) for doubly periodic functions with zero averages. Then the streamfunction and velocity can be recovered from the vorticity via

$$\psi(\mathbf{r}) = \int_{\mathcal{D}} G(\mathbf{r}, \mathbf{r}')\omega(\mathbf{r}')\,\mathrm{d}\mathbf{r}' \tag{2}$$

and

$$\mathbf{v}[\omega](\mathbf{r}) = \int_{\mathcal{D}} \mathbf{e}_z \times \nabla_{\mathbf{r}'} G(\mathbf{r}, \mathbf{r}')[q(\mathbf{r}') - h(\mathbf{r}')]\,\mathrm{d}\mathbf{r}', \tag{3}$$

respectively. Here we explicitly define the operator $\mathbf{v}[\omega]$ that allows us to compute the velocity from the vorticity. Due to the double periodicity, it is convenient to consider a Fourier representation of the potential vorticity:

$$q(\mathbf{r}, t) = \sum_{\mathbf{k}} q_{\mathbf{k}}(t)\mathbf{e}_{\mathbf{k}}(\mathbf{r}), \tag{4}$$

where $\mathbf{e}_{\mathbf{k}}(\mathbf{r}) = \exp(i\mathbf{k} \cdot \mathbf{r}) / (L_x L_y)^{1/2}$ is the orthonormal Fourier basis for a doubly periodic domain. We introduce a stochastic noise η, defined as a sum of random noises

$$\eta(\mathbf{r},\,t) = \sum_{\mathbf{k}} f_{\mathbf{k}}\eta_{\mathbf{k}}(t)\,\mathbf{e}_{\mathbf{k}}(\mathbf{r}), \tag{5}$$

where $\eta_{\mathbf{k}}$ are independent, white in time real random noises, such that $\mathbb{E}\left[\eta_{\mathbf{k}}(t)\eta_{\mathbf{k}'}(t')\right] = \delta_{\mathbf{k},\mathbf{k}'}\delta(t-t')$, and $f_{\mathbf{k}}$ is a complex noise spectrum with randomized phases for each Fourier mode $\mathbf{k}$. Consequently, we can define the noise correlation as $\mathbb{E}[\eta(\mathbf{r},\,t)\eta(\mathbf{r}',\,t')] = C(\mathbf{r},\,\mathbf{r}')\delta(t-t')$, where $C(\mathbf{r},\,\mathbf{r}')$, the noise correlation matrix, can alternatively be represented in Fourier space in terms of the complex noise spectrum: $C(\mathbf{r}) = \sum_{\mathbf{k}} C_{\mathbf{k}}\,\mathbf{e}_{\mathbf{k}}(\mathbf{r})$ $= \sum_{\mathbf{k}}|f_{\mathbf{k}}|^2\mathbf{e}_{\mathbf{k}}(\mathbf{r})$. The noise amplitude σ can be associated with the energy injection rate through the normalization of the noise spectrum by

$$\frac{1}{2}\sum_{\mathbf{k}}\frac{C_{\mathbf{k}}}{k^2} = 1, \tag{6}$$

where $k = |\mathbf{k}|$ is the wavenumber of the wave vector $\mathbf{k}$.

The barotropic quasi-geostrophic model (1) on a doubly periodic domain conserves the energy

$$\mathcal{E}[\omega] = -\frac{1}{2}\int_D \omega\,\psi\,\mathrm{d}\mathbf{r}, \tag{7}$$

and, if the topology satisfies the condition $\int_D h(\mathbf{r})\,\mathrm{d}\mathbf{r} = 0$, an infinite number of Casimir functionals

$$\mathcal{C}_s[q] = \frac{1}{2}\int_D s(q)\,\mathrm{d}\mathbf{r}, \tag{8}$$

where $s(q)$ is any smooth function of the potential vorticity q. On the other hand, a common choice of topography corresponds to the beta-plane approximation $h(\mathbf{r}) = \beta y$. This model is widely used as a simple model for atmospheric and ocean flows, where the curvature of the Earth is approximated by a beta-plane [37]. The beta-plane approximation $h(\mathbf{r}) = \beta y$ does not satisfy the condition $\int_D h(\mathbf{r})\,\mathrm{d}\mathbf{r} = 0$, and so an infinite number of Casimirs are not conserved. However, the quadratic Casimir $s(q) = q^2/2$ (in addition to the energy (7)) is conserved. In any case, all the models discussed above—the barotropic quasi-geostrophic model on a beta-plane and the one-layer quasi-geostrophic model, including the two-dimensional Navier–Stokes equations—conserve two sign-definite quadratic invariants: the energy (7) and the enstrophy (the quadratic Casimir) $\mathcal{C}_2[q] = (1/2)\int_D q^2\,\mathrm{d}\mathbf{r}$ (where $q = \omega$ for the Navier–Stokes case). Due to the presence of two quadratic invariants, a simple phenomenological argument [38] shows that energy will flow to large scales, whereas the enstrophy travels toward small scales. The implications of inverse energy transfer are of paramount importance in atmospheric and ocean flows. Restrictions imposed by finite-size domains lead (in the inertial limit) to the condensation of energy at the largest scales, which in turn causes the self-organization of the flow into large-scale coherent structures on a background of random turbulent fluctuations. The explicit form of these structures depends explicitly on the boundary conditions and on the noise correlation. For periodic boundary conditions, coherent structures in the inertial limit of the Navier–Stokes (Euler) equations can take the form of a vortex dipole or zonal jets [35], whereas only zonal jets are observed in large β regimes of the barotropic quasi-geostrophic model [39, 40].

Using the definition of energy (7) and the equation of motion (1), we can derive an equation for the energy balance in the system. By taking the scalar product of (1) with the streamfunction ψ and integrating, and applying Itô's lemma to the noise, we arrive at

$$\frac{\partial\mathcal{E}}{\partial t} = -2\alpha\mathcal{E} - \nu\mathcal{H} + \sigma, \tag{9}$$

where $\mathcal{H} = \int_D \psi(-\Delta)^n\omega\,\mathrm{d}\mathbf{r}$ corresponds to the dissipation of energy via the hyperviscosity term. Assuming the system has achieved a non-equilibrium steady state such that the system reaches an energy balance between the injection σ and the dissipation, and by further assuming that the majority of the energy is concentrated at the largest scales (meaning that it is reasonable to neglect energy dissipation through the hyperviscous term $\mathcal{H}$), we can perform a non-dimensionalization to fix the mean energy density to be of order one. By enforcing that the mean energy density be unity, i.e., that $\mathcal{E}/L^2 = U^2 = L^2/\tau^2 = 1$, where τ is now the characteristic energy turnover time at the domain scale L, from the energy balance equation (9) and assuming steady-state conditions ($\partial\mathcal{E}/\partial t = 0$), we can estimate the typical energy turnover timescale as $\tau = (2\alpha L^4/\sigma)^{1/2}$. Then, by non-dimensionalizing with respect to this timescale, we define new non-dimensional variables as $t' = t\tau, \omega' = \omega\tau$, $h'(\mathbf{r}) = h(\mathbf{r})\tau, \alpha' = \alpha\tau, \nu' = \nu\tau/L^{2n}$, and $\eta' = \eta L^2\tau^{1/2}$, resulting in the barotropic model in non-dimensional form:

$$\frac{\partial q'}{\partial t'} + \mathbf{v}'\cdot\nabla q' = -\alpha'\omega' - \nu'(-\Delta)^n\omega' + \sqrt{2\alpha}'\eta', \tag{10a}$$

$$\mathbf{v}' = \mathbf{e}_z \times \nabla\psi', \qquad q' = \omega' + h'(\mathbf{r}) = \Delta\psi' + h'(\mathbf{r}), \tag{10b}$$

From this moment on, we will deal with the non-dimensionalized quasi-geostrophic equation (10) with all primes dropped.

2.1. Dynamics of the statistically steady state

For turbulent regimes where the flow is dominated by the presence of large-scale coherent structures, we consider the inertial limits of the barotropic quasi-geostrophic equation (10): $\nu < \alpha < 1$. The type of coherent structures observed is dependent on the topography $h(\mathbf{r})$. Much work has been done in the inertial (Euler) limit, where $h(\mathbf{r}) = 0$. Here the main approach has been to advocate the timescale separation between the inertial dynamic and the slow dissipative and noise dynamics. It follows that the invariant measure will concentrate close to the attractors of the two-dimensional Euler equations. A set of attractors can be found using equilibrium statistical mechanics in the form of the Miller–Roberts–Sommeria theory through an energy–Casimir variational problem [41, 42]. The theory predicts the formation of either a large-scale vortex dipole or a two-band zonal jet. The appearance of the vortex dipole is associated with the degeneracy of the two smallest eigenfunctions of the Laplace operator of the square geometry. For $h(\mathbf{r}) \neq 0$, the picture is a little more complicated. If we consider the barotropic model on a beta-plane, where $h(\mathbf{r}) = \beta y$, then the relevant physical parameter that determines the type of coherent structures observed is β. For $\beta < 1$, we have the usual Euler (or Navier–Stokes) equations, where we expect to observe the invariant measure to concentrate close to vortex dipoles or zonal jets [35]. For rectangular domains, stable parallel flows are formed along the largest scales, where two jets appear in opposite directions. For $\beta > 1$, the β-effect dominates, which tends to stabilize the parallel flows in the $\mathbf{e}_x$ (zonal) direction (corresponding to the smallest eigenfunction). Then possible steady-state solutions to the barotropic equations with more than two jets can be observed. A rough estimate of the number of jets observed can be made by considering the ratio of the domain size L to the Rhine's scale given by $L_\beta = 1/\beta\tau$. However, it must be stated that this is only an approximate measure because the structure of the noise correlation will also contribute. Moreover, many cases of multiple steady-state solutions of the barotropic equation with differing numbers of jets have been observed for the same sets of parameters [36]. These multiple states are assumed to be linearly stable for the unforced (with or without dissipation) dynamics. Consequently, when one introduces stochastic fluctuations by the addition of a noise, the dynamical attractors become meta-stable, and one may expect to observe rare transitions between several attractors.

2.2. The large deviation and instanton approach

Transitions between coexisting attractors and the appearance of uncommon large-scale flows are rare events. There are many ways in which one can study these rare events in general. However, one of the most promising is the large deviation and instanton approach. This strategy relies on the description of the transition probability of observing a transition between two states in terms of a Feynman path integral derived from the statistical properties of the noise [43]. For simplicity, one usually assumes that the system is driven by a white in time noise; however, attempts have been made to generalize the formalism to include colored noises [44]. Detailed mathematical derivations of the transition probability can be found in classical textbooks [29, 30]. The final result is an Onsager–Machlup path integral [45, 46] over all possible transition trajectories from a state q_0 to a state q_T occurring in time T, where each transition is weighted according to some action functional $\mathcal{A}$:

$$P\Big[q_T,\, T;\, q_0,\, 0\Big] \;=\; \int_{q(0)=q_0}^{q(T)=q_T} \exp\left(-\frac{\mathcal{A}_{(0,T)}[q]}{2\alpha}\right)\mathcal{D}[q]. \tag{11}$$

Here deviations from the zero noise (deterministic) relaxation trajectory are represented by a penalty function defined through an action functional $\mathcal{A}_{(0,T)}[q]$. The action is the time integral of the Lagrangian associated with the dynamical equations:

$$\mathcal{A}_{(0,T)}[q] = \int_0^T \mathcal{L}\left[q, \frac{\partial q}{\partial t}\right]\mathrm{d}t. \tag{12}$$

For the barotropic quasi-geostrophic equation (10), the Lagrangian is explicitly

$$\begin{aligned}\mathcal{L}\left[q, \frac{\partial q}{\partial t}\right] = \frac{1}{2}\int_{\mathcal{D}}\int_{\mathcal{D}}\left[\frac{\partial q}{\partial t} + \mathbf{v}\cdot\nabla q + \alpha\omega + \nu(-\Delta)^n\omega\right](\mathbf{r}) \\ \times C^{-1}(\mathbf{r},\,\mathbf{r}')\left[\frac{\partial q}{\partial t} + \mathbf{v}\cdot\nabla q + \alpha\omega + \nu(-\Delta)^n\omega\right](\mathbf{r}')\,\mathrm{d}\mathbf{r}\mathrm{d}\mathbf{r}',\end{aligned} \tag{13}$$

where $C^{-1}(\mathbf{r},\,\mathbf{r}')$ is the formal inverse of the noise correlation, such that $\int_{\mathcal{D}} C(\mathbf{r},\,\mathbf{r}_1)C^{-1}(\mathbf{r}_1,\,\mathbf{r}')\,d\mathbf{r}_1 = \delta(\mathbf{r}-\mathbf{r}')$.

For rare probabilities, the path integral is a Laplace integral, and one can often perform a saddle-point approximation around the global minimum of the action functional to get a leading-order approximation of the

transition probability. This estimate will be based on the action of the trajectory that globally minimizes the action functional. This global minimizer will be the most probable transition path going from state q_0 to q_T in time T. At its most simple, it will consist of the most probable fluctuation path out of the initial attractor to the edge of the basin of attraction of a neighoring attractor (known as an instanton) and then the relaxation to the second attractor. Mathematically, this is defined as

$$q^\star(t) = \underset{\{q \mid q(\mathbf{r},0)=q_0,\, q(\mathbf{r},T)=q_T\}}{\arg\min} \mathcal{A}_{(0,T)}[q]. \tag{14}$$

When the saddle-point approximation is valid, the transitions are rare and are clustered around the instanton path. As global minima, the most probable paths are critical points of the action functional (12) and satisfy the corresponding Euler–Lagrange equations

$$\frac{\delta \mathcal{L}}{\delta q} = \frac{d}{dt}\frac{\delta \mathcal{L}}{\delta \dot{q}}, \tag{15}$$

where $\dot{q} = \partial q/\partial t$. The Euler–Lagrange equation (15) can be re-expressed in terms of an instanton Hamiltonian $\mathcal{H}[q, p]$ for canonical variables q and $p = \delta\mathcal{L}/\delta\dot{q}$[3]:

$$\frac{\partial q}{\partial t} = \frac{\delta \mathcal{H}}{\delta p}, \tag{16a}$$

$$\frac{\partial p}{\partial t} = -\frac{\delta \mathcal{H}}{\delta q}. \tag{16b}$$

The instanton Hamiltonian is a quantity that remains conserved by the dynamics of the most probable transition path (instanton and relaxation). Therefore, $\mathcal{H}$ becomes an extremely useful quantity for numerical purposes, where it can be used to determine whether a transition path is a critical point of the action functional (12). For the quasi-geostrophic dynamics (10) the instanton Hamiltonian $\mathcal{H}$ is given by

$$\mathcal{H}[q, p] = \frac{1}{2}\int p(\mathbf{r})\, C(\mathbf{r}, \mathbf{r}')\, p(\mathbf{r}')\, \mathrm{d}\mathbf{r}\mathrm{d}\mathbf{r}' - \int p(\mathbf{r})\Big[\mathbf{v}\cdot\nabla q + \alpha\omega + \nu\left(-\Delta^n\right)\omega\Big](\mathbf{r})\, \mathrm{d}\mathbf{r}. \tag{17}$$

Then the Euler–Lagrange equations become explicitly

$$\frac{\partial p}{\partial t} + \mathbf{v}\cdot\nabla p = \Delta^{-1}\left(\mathbf{e}_z\cdot[\nabla q\times\nabla p]\right) + \alpha p + \nu(-\Delta)^n p, \tag{18a}$$

$$\frac{\partial q}{\partial t} + \mathbf{v}\cdot\nabla q = -\alpha\omega - \nu(-\Delta)^n\omega + \int_{\mathcal{D}} C(\mathbf{r}, \mathbf{r}')\, p(\mathbf{r}')\, \mathrm{d}\mathbf{r}', \tag{18b}$$

subject to the boundary conditions $q(\mathbf{r}, 0) = q_0$ and $q(\mathbf{r}, T) = q_T$. The Euler–Lagrange equation (18) are also known as the instanton equations because the most probable transition path will satisfy them. It should be made clear that any transition path that is a critical point of the action functional may satisfy the Euler–Lagrange equation (18), not only the most probable one (14). On general grounds, one should expect multiple solutions to the instanton equations, hence leading one to compare their respective action values in order to determine the most likely path. It should be emphasized that equations (18) are valid only in the Freidlin–Wentzell limit of the transition being rare, where the saddle-point approximation is valid.

A straightforward study of rare transitions through direct numerical simulation of the governing equations is nearly always impracticable. This is mainly a complexity problem, due to the large number of degrees of freedom involved for genuine turbulent flows and the extremely long time between two successive transitions. The path integral approach provides a way to systematically determine the most likely transition path between two attractors. Through the action functional $\mathcal{A}$ with the *a priori* given attractors, one can predict the most probable rare transition by considering the local action minimizers or by solving the instanton equations with appropriate boundary conditions. Theoretically, this problem is also extremely difficult and, for turbulent flows, can be achieved only in the simplest of circumstances (see section 5). Alternatively, one can resort to numerical approaches. Numerical algorithms exist that compute the most probable transition paths by iteratively converging toward local action minimizers (see section 4) or by directly solving the boundary value problem associated with the instanton equations (18) (for instance, see [47]).

In the cases where the dynamics are in equilibrium, i.e., where they satisfy Langevin dynamics, every transition out of an attractor can be rare. This allows for the direct computation of rare transitions through deterministic relaxation trajectories in a related dual system [28], as will be discussed in the next section.

[3] The instanton Hamiltonian is conserved because it is actually the value of the Hamiltonian that corresponds to the time-invariant action minimization, as in any classical mechanics problem. The instanton Hamiltonian structure derived through the action minimization should not be confused with the Hamiltonian structure of the two-dimensional Euler equations.

3. Equilibrium Langevin dynamics of the two-dimensional quasi-geostrophic equations

This section contains a brief overview of recent theoretical work [28] on the Langevin dynamics of the quasi-geostrophic equations. We introduce the Langevin dynamics description for the quasi-geostrophic equations, where a specific relationship between the noise correlation and the kernel of the potential force invokes the Langevin property. By specifying a particular structure of the potential term, we consider a Langevin dynamics with a first-order phase transition between coexisting zonal flow attractors. Through the equilibrium Langevin dynamics theory, we can analytically predict the most probable rare transition paths between two attractors by considering an effective potential landscape and relaxation (unforced) trajectories of a dual dynamics. This also yields an Arrhenius law for the transition probability. The final part of this section is dedicated to the direct numerical simulations of the bistable system considered in [28], verifying numerically that the theoretical predictions hold.

3.1. The two-dimensional quasi-geostrophic Langevin equations

The Langevin formalism was previously considered for the two-dimensional quasi-geostrophic and Euler equations in [28]. We explain why the two main hypotheses of Langevin dynamics (Liouville property and conservation of the potential related to the transversality condition) are verified when the kernel in front of the gradient part and the noise autocorrelation are identical.

The Langevin dynamics associated with the quasi-geostrophic equations in a periodic domain $\mathcal{D} = [0,\, 2\pi\delta) \times [0,\, 2\pi)$ with aspect ratio δ are given by

$$\frac{\partial q}{\partial t} + \mathbf{v}[q-h]\cdot\nabla q = -\alpha\int_D C(\mathbf{r},\mathbf{r}')\frac{\delta\mathcal{G}}{\delta q(\mathbf{r}')}\,\mathrm{d}\mathbf{r}' + \sqrt{2\alpha\gamma}\,\eta, \tag{19a}$$

$$\mathbf{v} = \mathbf{e}_z\times\nabla\psi, \quad \omega = \Delta\psi, \quad q = \omega + h(\mathbf{r}), \tag{19b}$$

with potential $\mathcal{G}$. The stochastic force η is a Gaussian process, white in time, with correlation function $\mathbb{E}[\eta(\mathbf{r},\,t)\eta(\mathbf{r}',\,t')] = C(\mathbf{r},\,\mathbf{r}')\delta(t-t')$. The topography $h(\mathbf{r})$ is such that $\int_D h(\mathbf{r})\,\mathrm{d}\mathbf{r} = 0$, and we also introduce a new parameter γ that will control the strength of the noise relative to the potential term. For the Langevin description to be correct, the potential $\mathcal{G}$ must consist of conserved quantities of the inviscid ($\alpha = 0$) dynamics of (10). Moreover, the deterministic equations for Langevin dynamics (equations (19) for $\alpha = 0$) essentially correspond to a transport equation by a non-divergent velocity field, leading to a Liouville property for the nonlinear advection term $\mathbf{v}\cdot\nabla q$. A more detailed discussion of the Langevin assumptions and results can be found in [28].

As with the quasi-geostrophic equation (10), the equilibrium quasi-geostrophic dynamics conserve the energy $\mathcal{E}$ and an infinite number of Casimirs $\mathcal{C}_s$ given by equations (7) and (8) respectively for the deterministic ($\alpha = 0$) dynamics. It follows that the correct choice of the potential $\mathcal{G}$ for Langevin dynamics will consist of a combination of these conserved quantities:

$$\mathcal{G} = \mathcal{C}_s + \beta\mathcal{E}. \tag{20}$$

3.2. Reversed dynamics and the relaxation equation

For the two-dimensional Euler or quasi-geostrophic equations, the time-reversed dynamics defined as $q_r(t) = I[q(T-t)]$ also satisfies a Langevin dynamics through a set of symmetries with the relevant involution operator $I[\cdot]$ corresponding to a time reversal being

$$I[q] = -q. \tag{21}$$

Then the dual process is given by (19) but with $\mathbf{v}[q-h]\cdot\nabla q \to \mathbf{v}[q+h]\cdot\nabla q$, where the velocity operator is defined by equation (3) and $\mathcal{G}[q] \to \mathcal{G}[-q]$, giving

$$\frac{\partial q}{\partial t} + \mathbf{v}[q+h]\cdot\nabla q = -\alpha\int_D C(\mathbf{r},\mathbf{r}')\frac{\delta\mathcal{G}[-q]}{\delta q(\mathbf{r}')}\,\mathrm{d}\mathbf{r}' + \sqrt{2\alpha\gamma}\,\eta, \tag{22a}$$

$$\mathbf{v} = \mathbf{e}_z\times\nabla\psi, \quad \omega = \Delta\psi, \quad q = \omega - h(\mathbf{r}). \tag{22b}$$

We observe that for the two-dimensional Euler equations ($h = 0$), the dual dynamics (22) agree with the original dynamics (19) if the potential $\mathcal{G}$ is even. Then we conclude that the dynamics are time-reversible and detailed balance is verified. If, however, $\mathcal{G}$ is not even or $h \neq 0$, then the dynamics are not time-reversible and the original dynamics are conjugate to another Langevin dynamics where h has to be replaced by $-h$ and $\mathcal{G}[q]$ by $\mathcal{G}[-q]$. In this case, detailed balance is not verified.

For Langevin dynamics, the instantons from one attractor to a saddle are given by the reverse of the relaxation paths of the corresponding dual dynamics. The relaxation paths are simply the deterministic

trajectories of the Langevin dynamics (19) with $\gamma = 0$. Therefore, for the barotropic quasi-geostrophic equations the equation for the relaxation paths is

$$\frac{\partial q}{\partial t} + \mathbf{v}[q+h] \cdot \nabla q = -\alpha \int_D C(\mathbf{r}, \mathbf{r}') \frac{\delta \mathcal{G}}{\delta q(\mathbf{r}')}[-q]\, \mathrm{d}\mathbf{r}'. \tag{23}$$

Equation (23)is known as the relaxation equation. It provides the means to directly compute, through deterministic means, the instanton trajectories from an attractor to a saddle by considering the relaxation paths, defined by (23), from the saddle to the attractor.

3.3. The energy–enstrophy ensemble and physical dissipation

A special case of Langevin dynamics occurs when the potential is given by the following form:

$$\mathcal{G} = \int_D \frac{(q-h)^2}{2}\, \mathrm{d}\mathbf{r} + \beta \mathcal{E}. \tag{24}$$

This structure is referred to as the potential enstrophy ensemble (when $\beta = 0$), the enstrophy ensemble (when $\beta = 0$ and $h = 0$), or generally as the energy–enstrophy ensemble. The properties of the corresponding invariant measures have been discussed on a number of occasions, starting with the works of Kraichnan [48] in the case of Galerkin truncations of the dynamics, and for some cases without discretization; see, for instance, [49] and references therein.

For specific choices of the potential $\mathcal{G}$ and of the noise correlation C, the friction term can also be identified with a classical physical dissipation mechanism. For instance, if $C(\mathbf{r}, \mathbf{r}') = \Delta\delta(\mathbf{r} - \mathbf{r}')$, and the potential takes the form of (24), then the dissipative term on the right-hand side of (19) is

$$-\alpha \int_D C(\mathbf{r}, \mathbf{r}') \frac{\delta \mathcal{G}}{\delta q(\mathbf{r}')}[q]\, \mathrm{d}\mathbf{r}' = \alpha\Delta\omega - \alpha\beta\omega, \tag{25}$$

which leads to diffusion-type dissipation with viscosity α and linear friction with friction parameter $\alpha\beta$ for the vorticity $\omega = q - h$. Such linear friction can model the effects of three-dimensional boundary layers on the quasi two-dimensional bulk vorticity, which appear in experiments with a very large aspect ratio, rotating tank experiments, and soap film experiments.

The fact that for the enstrophy ensemble, the quasi-potential is simply the enstrophy, the relaxation and fluctuation paths can be easily computed explicitly in many scenarios, as is discussed in [35].

For the majority of the other cases, the dissipative term on the right-hand side of (19) cannot be identified as a microscopic dissipation mechanism or as a physical mechanism. There is, however, another possible interpretation of this kind of friction term. As explained in [50], entropy maxima subjected to constraints related to the conservation of energy and the distribution of vorticity are also extrema of energy–Casimir functionals. By analogy with the Allen–Cahn equation in statistical mechanics, which uses the free energy as a potential, it seems reasonable to describe the largest scales of turbulent flows as evolving through a gradient term of the energy–Casimir functional. Such models have been considered in the past. (See, for example, [51, 52] and references therein.) At this stage, this should be considered a phenomenological approach, as no clear theoretical results exist to support this view.

3.4. Phase transitions and instantons between zonal flows in the equilibrium quasi-geostrophic equations

To fully determine the quasi-geostrophic Langevin dynamics (19), we need to specify the topography function and the potential $\mathcal{G}$. Given the infinite number of conserved quantities for the quasi-geostrophic dynamics, there are many possible choices. We are interested in the description of the phenomenology of phase transitions and instanton theory in situations of first-order transitions. Therefore, we will illustrate such a phenomenology through an example originally discussed in [28].

As an illustrative example, we choose a zonal topography (depending only on y) given by $h(\mathbf{r}) = H\cos(2y)$ on a periodic domain $[0,\ 2\pi\delta) \times [0,\ 2\pi)$. For this simple choice, the attractors will be zonal flows (jets), similar to the dynamics of planetary atmospheres, such as, for instance, that of Jupiter. The fact that the attractors are purely zonal makes this example one of the simplest possible and more easily amenable to further theoretical study. Consequently, the potential vorticity is given by

$$q = \Delta\psi + H\cos(2y). \tag{26}$$

We consider the potential

$$\mathcal{G} = \mathcal{C} + \beta\mathcal{E}, \tag{27}$$

with energy $\mathcal{E}$ (equation (7)), with β being the inverse temperature, and where C is the Casimir functional:

$$C = \int_D \frac{q^2}{2} - \epsilon\frac{q^4}{4} + a_6\frac{q^6}{6}\,\mathrm{d}\mathbf{r}, \tag{28}$$

where we assume that $a_6 > 0$ and $\beta = -1 + \epsilon$. The choice of Casimir functional is due to the very interesting phase diagram that be can studied analytically in the limit of small ϵ [28]. For this analysis, using a Lyapunov–Schmidt reduction, we refer the reader to [28, 53].

In [28], it was shown that for the potential (27), with small β and $\epsilon > 0$ we expect to observe a first-order phase transition. When $H = 0$, a bifurcation occurs for $\beta = -1$ ($\epsilon = 0$), which can be easily verified (see [53]). This bifurcation is due to the vanishing of the Hessian at $\beta = -1$ ($\epsilon = 0$). As discussed in many papers [35, 53–55], for the quadratic Casimir functional $C_2 = \int_D q^2/2\,\mathrm{d}\mathbf{r}$, the first bifurcation involves the eigenfunction of $-\Delta$ with the lowest eigenvalue. If we assume that the aspect ratio $\delta < 1$, then the smallest eigenvalue is the one corresponding to the zonal mode proportional to $\cos(y)$. Because we are interested in transitions between two zonal states, we assume from now on that $\delta < 1$.

For nonzero but sufficiently small H, there will still be a bifurcation for ϵ close to zero. This is the regime that we want to consider. The null space of the Hessian is spanned by the eigenfunctions $\cos(y)$ and $\sin(y)$; therefore, as a consequence, for small enough ϵ and H, we expect that the bifurcation can be described by a normal form involving only the projection of the field q onto the null space. It was shown in [28] that by tackling the problem perturbatively, assuming that $\epsilon \ll 1$, $H^2 \ll 1$, and $a_6H^2 \ll \epsilon$, the Langevin dynamics can be described by an effective potential given by

$$\mathcal{G} = \delta\pi^2 G(A, B) \tag{29}$$

with G given at the leading order by

$$\begin{aligned} G(A, B) = &-\frac{H^2}{3} + \left(\epsilon - \frac{\epsilon H^2}{6} + \frac{5a_6H^4}{216}\right)\left(A^2 + B^2\right) \\ &+ \left(-\frac{3\epsilon}{8} + \frac{25a_6H^2}{144}\right)\left(A^2 + B^2\right)^2 + \frac{5a_6}{24}\left(A^2 + B^2\right)^3 + \frac{5a_6H^2}{72}\left(A^2 - B^2\right)^2, \end{aligned} \tag{30}$$

around the potential vorticity field of

$$q = -\frac{H}{3}\cos(2y) - A\cos(y) - B\sin(y) + \mathcal{O}(\epsilon) + \mathcal{O}\left(\epsilon A^2\right) + \mathcal{O}\left(a_6A^4\right). \tag{31}$$

The fact that G is a normal form for small enough ϵ, a_6, and H implies that the gradient of $\mathcal{G}$ in the directions transverse to $q = -A\cos(y) - B\sin(y)$ is much steeper than the gradient of G.

We observe that the term proportional to $\left(A^2 - B^2\right)^2$ breaks the symmetry between A and B. Its minimization imposes that $A^2 = B^2$. Then either $A = B$ or $A = -B$. If we take into account that minimizing with respect to $A^2 + B^2$ will give only the absolute value of A, we can surmise that we will have four equivalent nontrivial solutions:

$$q_i = -\frac{H}{3}\cos(2y) + \sqrt{2}\,|A|\,(\epsilon, a_6)\cos\left(y + \phi_i\right), \tag{32}$$

with ϕ_i taking one of the four values $\left\{-\frac{3\pi}{4}, -\frac{\pi}{4}, \frac{\pi}{4}, \frac{3\pi}{4}\right\}$, with $|A|$ minimizing:

$$\tilde{G}(|A|) = -\frac{H^2}{3} + 2\left(\epsilon - \frac{\epsilon H^2}{6} + \frac{5a_6H^4}{216}\right)|A|^2 + 4\left(-\frac{3\epsilon}{8} + \frac{25a_6H^2}{144}\right)|A|^4 + \frac{5a_6}{3}|A|^6. \tag{33}$$

The reduced potential G is plotted in figure 1 for the case $\epsilon > 0$. The structure has four nontrivial attractors due to a breaking of the symmetry imposed by the topography $h(y) = H\cos(2y)$. In figure 2, we present the potential vorticity across y of two of the four nontrivial attractors, the corresponding saddle between them, and the topography. Note that the other two nontrivial attractors (not shown) correspond to $y \to y \pm \pi$ translations arising from the $A \to -A$ symmetry of the two attractors displayed in figure 2.

Through the equilibrium hypothesis, we know how to describe and compute the instantons corresponding to the phase transitions between zonal flows. They are none other then the reversed trajectories for the relaxation paths for the dual dynamics. The corresponding equation of motion for the relaxation paths for the dual dynamics for the quasi-geostrophic dynamics is then derived in section 3.2.

In the current example, the potential $\mathcal{G}$ is an even function; see equation (28). Also, we remark that over the set of zonal flows $\mathbf{v} = U(y)\mathbf{e}_x$, the nonlinear term of the quasi-geostrophic equation vanishes: $\mathbf{v}[q + h] \cdot \nabla q = 0$. As a consequence, when the instanton remains a zonal flow, the fact that h has to be replaced

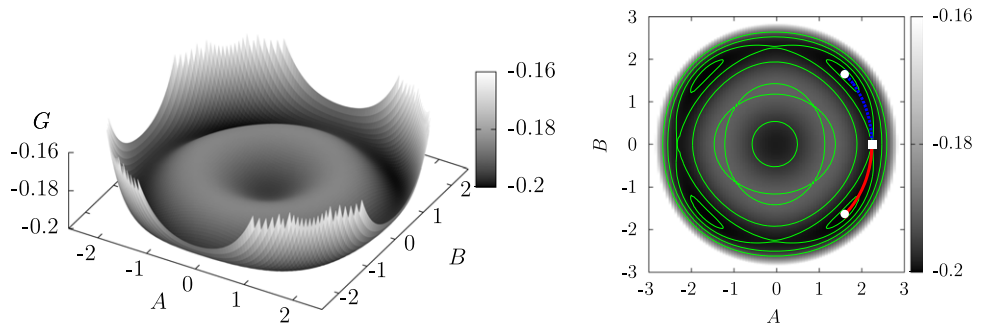

Figure 1. Figure adapted from [28]. Surface plot (left) and contour plot (right) of the reduced potential surface $G(A,\ B)$ (see equation (30)) for the parameters $\epsilon = 1.6 \times 10^{-2}, H = 7.746 \times 10^{-1}, a_6 = 2.6 \times 10^{-3}$. For these parameters, G has four global minima with $|A| = |B|$ and one local minimum at $A = B = 0$. This structure with four nontrivial attractors is due to symmetry breaking imposed by the topography $h(y) = H\ \cos(2y)$. Level contours are shown in green. The most probable transition path is shown by the red and blue curves. The instanton (red curve) is the reverse trajectory of a relaxation path from the saddle (white square) to the attractor (white circle).

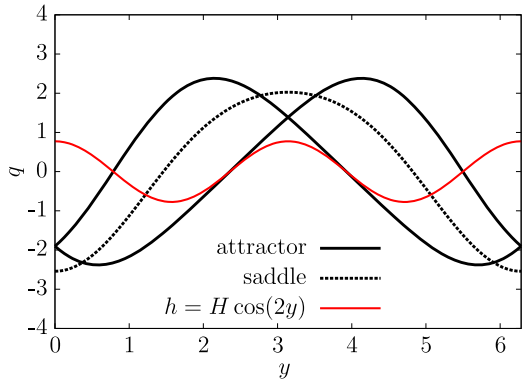

Figure 2. The plot depicts the topography $(h(y) = H\ \cos(2y)$, symmetric red curve) and two of the four nontrivial attractors of the potential vorticity q (solid black lines) corresponding to two minima of the effective potential G (see equation (30) and figure 1) for parameter value $\epsilon > 0$. In addition, we show the corresponding saddle between the two presented attractors (dashed black curve). The two other nontrivial attractors (not displayed) correspond to $y \to y \pm \pi$ translations of the ones shown.

by $-h$ has no consequence and hence the dynamics will be time-reversible. Let us now argue that the instanton is actually generically a zonal flow.

We assume for simplicity that the stochastic noise is homogeneous (invariant by translation in both directions). Then $C(\mathbf{r},\ \mathbf{r}') = C(\mathbf{r} - \mathbf{r}') = C_z(y - y') + C_m(y - y',\ x - x')$, where

$$C_z(y) = \frac{1}{2\pi\delta}\int_0^{2\pi\delta} C(x,\ y)\,\mathrm{d}x \tag{34}$$

is the zonal part of the correlation function and $C_m = C - C_z$ is the non-zonal or meridional part.

As the nonlinear term of the two-dimensional Euler equations identically vanishes, the relaxation dynamics has a solution among the set of zonal flows. If C_z is non-degenerate (positive definite as a correlation function), then relaxation paths will exist through the gradient dynamics

$$\frac{\partial q}{\partial t} = -2\pi\alpha\delta\int_0^{2\pi} C_z(y - y')\frac{\delta\mathcal{G}}{\delta q(y')}\,\mathrm{d}y', \tag{35}$$

where $q = q(y)$ is the zonal potential vorticity field.

Moreover, as argued previously, the fact that G (30) is a normal form for small enough a_6 and H implies that the gradient of $\mathcal{G}$ in directions transverse to $q = -A\ \cos(y) - B\ \cos(y)$ is much steeper than the gradient of G. As a consequence, at the leading order the relaxation paths will be given by the relaxation paths for the effective two degrees of freedom G. Then, from (29), (30), and (35), we obtain that, at the leading order, the dynamics of A and B are given by

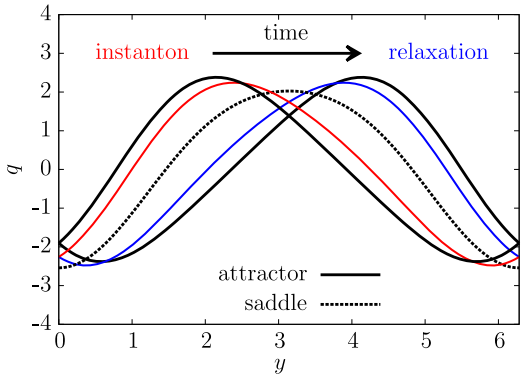

Figure 3. Figure adapted from [28]. The potential vorticity $q(y)$ for two of the nontrivial attractors (solid black curves), the corresponding saddle between the attractors (dashed black curve), and two intermediate profiles along the instanton path (solid red curve) and the relaxation path (solid blue curve).

$$\frac{\mathrm{d}A}{\mathrm{d}t} = -c\frac{\partial G}{\partial A} \quad \text{and} \quad \frac{\mathrm{d}B}{\mathrm{d}t} = -c\frac{\partial G}{\partial B}, \tag{36}$$

with $c = -\alpha\delta \int_0^{2\pi} C_z(y)\cos(y)\,\mathrm{d}y$, where we recall that G is given by equation (30).

From this result the relaxation paths are easily computed. Using the fact that fluctuation paths are time-reversed trajectories of relaxation paths, instantons are also easily obtained. One of the resultant relaxation paths (blue curve) and one of the instantons (red curve) are depicted in figure 1 overlapped on the contours of the potential G in the (A, B)-plane. The corresponding two attractors involved, together with the saddle point and examples of two intermediate states, are shown in figure 3.

For the Langevin dynamics formalism, the stationary probability distribution is known *a priori* and is given by

$$P_s[q] = \frac{1}{Z}\exp\left(-\frac{\mathcal{G}[q]}{\gamma}\right), \tag{37}$$

where Z is a normalization constant. At a formal level, this can be computed by easily writing the Fokker–Planck equation for the evolution of the probability density functional. Then the property that P_s is stationary readily follows from the Liouville theorem and the fact that $\mathcal{G}$ consists of the conserved quantities of the deterministic dynamics.

Subsequently, the transition rate k for rare transitions between two attractors is given by an Arrhenius law of the form

$$k = C\exp\left(\frac{\Delta\mathcal{G}[q]}{\gamma}\right), \tag{38}$$

where C is an order-one prefactor and $\Delta\mathcal{G} = \mathcal{G}[q_{\text{saddle}}] - \mathcal{G}[q_{\text{attractor}}]$ is the potential difference between the saddle and the initial attractor.

3.5. Direct numerical simulations of rare transitions between coexisting attractors

To verify the theoretical predictions of rare transitions in the equilibrium case, we perform direct numerical simulation of the Langevin example previously discussed.

We numerically solve the Langevin dynamics of the quasi-geostrophic equations given by (19) by using a pseudo-spectral spatial discretization scheme of resolution 64×128 on a periodic domain $[0,\ 2\pi\delta) \times [0,\ 2\pi)$ with $\delta = 1/2$. Due to aliasing errors from the quintic nonlinearity associated with potential $\mathcal{G}$, we fully dealias courtesy of a 2/6 rule [56]. We time-integrate the system using a second-order Runge–Kutta method with time step $\mathrm{d}t = 2 \times 10^{-3}$. For simplicity we choose a white in time noise with correlation $C(\mathbf{r}, \mathbf{r}') = \delta(\mathbf{r} - \mathbf{r}')/Z$, where Z is the normalization constant defined through condition (6). We add hyperviscous dissipation to the right-hand side of equation (19) (see equation (39)) to act as a small-scale regularization in order to avoid any numerical problems. The addition of this extra dissipation breaks the equilibrium hypothesis on a general basis. However, the dissipation acts only on the extremely high harmonics, with little effect on the dynamics of the largest scales. Therefore, we expect little deviation from the theoretical (equilibrium) prediction. The numerical equation of motion is

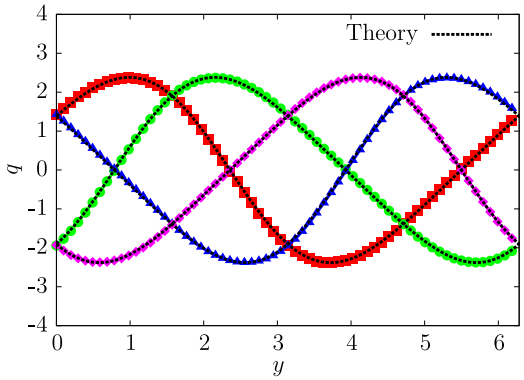

Figure 4. Numerical attractors found using the relaxation equation (23). The dashed black lines correspond to the global minima from the effect potential $G(A, B)$. The red, blue, green, and orange curves correspond to numerical solutions from equation (23).

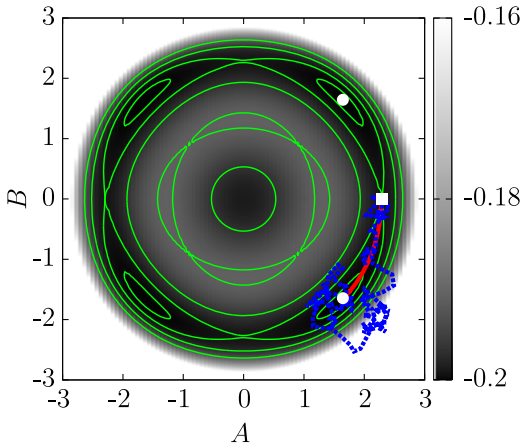

Figure 5. Rare transition from one attractor to the neighboring saddle, with $\gamma = 5 \times 10^{-2}$ (dashed blue curve) taken from direct numerical simulation of the system (39) overlaid over the contour plot of the effective potential landscape of figure 1 with the theoretically predicted instanton (solid red curve).

$$\frac{\partial q}{\partial t} + \mathbf{v}[q-h]\cdot\nabla q = -\frac{\alpha}{Z}\Big[q - \epsilon q^3 + a_6 q^5 - \beta\Delta^{-1}(q-h)\Big] + \nu(-\Delta)^n(q-h) + \sqrt{2\alpha\gamma}\,\eta, \tag{39a}$$

$$\mathbf{v} = \mathbf{e}_z \times \nabla\psi, \quad \omega = \Delta\psi, \quad q = \omega + h(\mathbf{r}). \tag{39b}$$

As an additional check of the predictions of subsection 3.4 we perform a relaxation of the system (39) from arbitrary initial conditions with $\nu = \gamma = 0$. From the effective potential landscape, the system should converge to the attractors of $\mathcal{G}$ given by (32). By starting at four different regions of phase space, we indeed find the predicted attractors of $\mathcal{G}$ plotted in figure 4. We observe that the theoretically predicted attractors (dashed black curves) overlay perfectly the numerically found attractors (colored curves).

From the numerical perspective, we initialize the system beginning from one of the attractors and time-step the system until we observe a transition to a neighboring saddle. We expect that if we are in a sufficiently weak noise limit $\gamma \ll \Delta\mathcal{G}$, the transition in the direct numerical simulation will remain close to the theoretically predicted instanton (red curve in figure 1). Therefore, we use the following parameters in our numerical simulation: $\alpha = 1 \times 10^{-1}, \nu = 1 \times 10^{-13,}$, and $\gamma = 5 \times 10^{-2}$.

In figure 5 we plot the numerically observed transition onto the contour plot of the effective potential G. We observe a relatively noisy transition (dashed blue curve) up to the saddle from the initial attractor. We see a lot of fluctuations at the base of the potential well where the gradients are small. As the transition progresses up the potential well toward the saddle, we observe better agreement with the theoretically predicted transition (solid red curve). We expect that closer agreement with the theoretically predicted transition would be observed if we chose a smaller γ, but at the cost of a far rarer transition. In principle, fluctuations around the instanton solution can be addressed with the path integral formalism from the functional expansion of the Onsager–Machlup action up to the second order with regard to fluctuations. However, such analysis goes beyond the scope of the current article.

4. Numerical optimization of the Onsager–Machlup action functional for the barotropic quasi-geostrophic equations

In this section we develop a numerical algorithm that computes local action minimizers of the Onsager–Machlup action functional defined in section 2. These local action minimizers are candidates for the most probable transition paths between two states. Unfortunately, these numerical optimization techniques are usually unable to distinguish between local minimizers and global ones. Therefore, using numerical schemes that are based on minimization of the action functional may not lead to the most likely transition path. However, one may devise strategies to check to a certain degree whether a local or global minimum is obtained by perturbing found minima to see if they minimize to an alternative path. If multiple minima exist, then comparison of the total action can be made. As already stated, the numerical prediction of rare events without brute force simulations, observation, or experiments is important. The advantage of the action minimization methods is that they can be applied to non-gradient systems in both equilibrium and non-equilibrium cases.

Alternative strategies exist to compute rare transitions, such as string methods [57, 58], the nudged elastic band method [59], eigenvector-following-type methods [60], the dimer method [61], and obtaining direct solutions to the instanton equation [62]. However, many of these methods cannot be applied to turbulent systems in general.

The numerical scheme that we implement here is based on adaption of the *minimum action method* to turbulent systems. In essence, this procedure uses a series of iterative estimates of transition paths until it finds a local minimum of the action functional $\mathcal{A}$. This numerical method is applicable to both the equilibrium and non-equilibrium cases and can easily be extended to consider more complex turbulence problems.

4.1. The minimum action method

The minimum action method is a class of numerical optimization procedures that determine local minimizers of functionals. One of the key properties of this algorithm is that it can be applied to systems that do not provide *a priori* an energy potential landscape. This makes it ideal for studying rare transitions in turbulence problems. It has already found many applications in the use of computing most probable transition paths in low-dimensional gradient systems [63, 64]and rare transitions in the the Kuramoto–Siavashinksky equation [65] and the Kardar–Parisi–Zhang equation [66]. In this section, we outline an algorithm for the standard minimum action method; however, many more advanced versions exist that may be useful in the future. These include algorithms that provide adaptive re-meshing known as *adaptive minimum action methods* [64, 67] or ones that use an arc length parameterization of time to compute infinite time transition paths, known as *geometric minimum action methods* [68, 69].

The generic strategy of the minimum action method algorithm is to begin with an initial estimate of the most probable transition path between two states. Then, with the use of variations of the action functional with respect to the transition trajectory, improvements in the form of iterations to the initial guess can be made that subsequently reduce the action. This iterative process is continually repeated until the series of estimates converges to a local minimum of the action functional.

The main complexity of this method is in determining how one should improve each guess so that the action is reduced. One can use various strategies, such as applying Newton's method [70], which uses information about the first and second variations (Hessian) of the action functional or quasi-Newton methods, such as the popular Broyden–Fletcher–Goldfarb–Sahnno (BFGS) scheme, which iteratively approximates the Hessian without the need to compute it directly. Newton's method is a relatively expensive procedure, especially for high-dimensional minimization problems, where the computation of the Hessian is difficult. Subsequently, quasi-Newton methods have been favored in the community and have been successfully applied to the minimum action method but only in situations involving low-dimensional gradient systems [63, 66].

We found that for turbulence problems, where we have to deal with a large number of degrees of freedom, even quasi-Newton methods are expensive. Therefore, we are obliged to resort to relying on methods based solely on using the first variation of the action functional. The simplest method that falls into this category is the method of steepest descent, where a descent direction d is taken in the direction of the local anti-gradient of the action functional, i.e., $d = -\delta\mathcal{A}/\delta q$. Usually these methods can have poor convergence rates when the potential energy landscape consists of long, narrow valleys, where the minimization procedure leads to zig-zagging across the narrow valley rather than along it. To improve convergence in these situations, one can use the nonlinear conjugate gradient method, which uses knowledge about previous descent steps to avoid crossing back and forth across potential valleys [70]. It is with this in mind that we use a nonlinear conjugate gradient method for our problem.

For our notation, we label each iteration with a superscript such that the nth estimate of the most probable transition path is labeled q^n for $n = 0,\ 1,\ 2,\ldots$. The initial guess is denoted as q^0. Each new estimate for the most

probable transition path q^{n+1} is computed from the previous guess q^n by taking an appropriate descent step of size l^n in the descent direction d^n:

$$q^{n+1} = q^n + l^n d^n. \tag{40}$$

The descent direction d^n is obtained through a nonlinear conjugate gradient method [70]. In general, for nonlinear conjugate gradient methods one takes the descent direction as

$$d^{n+1} = -\frac{\delta \mathcal{A}}{\delta q^n} + \beta^n d^n \quad \text{where} \quad d^0 = -\frac{\delta \mathcal{A}}{\delta q^0}. \tag{41}$$

The parameter β^n is known as the nonlinear conjugate gradient parameter, and it determines to what extent the current descent direction should depend on the previous descent direction. There are various ways of computing β^n, but we found that the most optimal was to use the standard Fletcher and Reeves formula, where

$$\beta^n = \frac{\left|\left|\frac{\delta \mathcal{A}}{\delta q^n}\right|\right|^2}{\left|\left|\frac{\delta \mathcal{A}}{\delta q^{n-1}}\right|\right|^2}, \tag{42}$$

where $||\cdot||$ is an appropriate norm. Due to the finite number of degrees of freedom associated with the numerical discretization, there can only be a finite number of orthogonal descent directions. Therefore, it will become important to occasionally reset the nonlinear conjugate gradient parameter when two consecutive descent directions are far from being orthogonal. To achieve this, we set $\beta^n = 0$, resulting in a standard steepest descent step when

$$\frac{\left(\frac{\delta \mathcal{A}}{\delta q^n}, \frac{\delta \mathcal{A}}{\delta q^{n-1}}\right)}{\left|\left|\frac{\delta \mathcal{A}}{\delta q^{n-1}}\right|\right|^2} > 0.5, \tag{43}$$

where $(\cdot, \cdot)$ is the inner product associated with the norm $||\cdot||$.

The step length l^n is chosen such that we obtain the the greatest reduction in the action functional. To ensure that d^n corresponds to a descent direction (that it results in the reduction of the action), the step length l^n must satisfy the strong Wolfe conditions [70]. Fortunately, standard line search algorithms exist for determining the largest step length that satisfies the strong Wolfe conditions. Therefore, we implement the line search algorithm 3.5 of chapter 3 in [70].

The minimization is continuously performed for each iteration until the estimate of the most probable transition trajectory q^n is within some tolerance, say ϵ, of being a solution to the Euler–Lagrange equation (18). This is verified by halting the algorithm if the solution satisfies the condition

$$\left|\left|\frac{\delta \mathcal{A}}{\delta q^n}\right|\right| < \epsilon. \tag{44}$$

4.2. Numerical discretization of the action functional

To numerically minimize the action functional, we must first discretize the action in both time and space. Due to the periodicity of our domain, it is natural for us to consider the Fourier harmonics as the standard basis. In time, we approximate the transition on a uniform grid of $N_t + 1$ points along the interval $[0,\ T]$. All spatial derivatives are computed in Fourier space with the nonlinear terms computed in physical space using the 2/3 dealiasing rule (the standard pseudo-spectral method [56]). Derivatives in time are achieved by applying the second-order central finite difference scheme to a staggered grid labeled by $\{j + 1/2\}$ for $j = 0, \ldots, N_t - 1$, where time is parameterized by $t_j = j\Delta t$ for $j = 0, \ldots, N_t$ and $\Delta t = T/N_t$.

In this respect, the transition trajectory is fully represented by the set of Fourier amplitudes $\{q_{\mathbf{k},j}\} \equiv \{q_{\mathbf{k}}(j\Delta t)\}$ given by equation (4), for $j = 0, \ldots, N_t$ and $\mathbf{k} = \left(2\pi n_x/L_x,\ 2\pi n_y/L_y\right)$ for $n_{x,y} \in \left\{-N_{x,y}/2, \ldots, N_{x,y}/2 - 1\right\}$, where $N_x \times N_y$ is the spatial resolution. Due to the reality of the potential vorticity q, the Fourier harmonics satisfy the condition $q_{\mathbf{k}} = q^*_{-\mathbf{k}}$ at every point in time.

Using this convention, we define the numerically discretized action functional $A[q]$ as

$$A[q] = \frac{\Delta t}{2}\sum_{j=0}^{N_t}\sum_{\mathbf{k}}\frac{\left|\dot{q}_{\mathbf{k},j+\frac{1}{2}} + (\mathbf{v}\cdot\nabla q)_{\mathbf{k},j+\frac{1}{2}} + \alpha\omega_{\mathbf{k},j+\frac{1}{2}} + \nu k^{2n}\omega_{\mathbf{k},j+\frac{1}{2}}\right|^2}{\left|f_{\mathbf{k}}\right|^2}, \tag{45}$$

where we have used the notation $\dot{q}_{\mathbf{k},j+\frac{1}{2}} \equiv (q_{\mathbf{k},j+1} - q_{\mathbf{k},j})/\Delta t$ to denote the time derivative defined on the staggered grid. As a consequence, we must also compute the linear and nonlinear terms on the same grid. To do this, we average the contribution of neighboring points by the simple interpolation $q_{\mathbf{k},j+1/2} = (q_{\mathbf{k},j+1} + q_{\mathbf{k},j})/2$.

To compute the first variation of the action functional $\delta\mathcal{A}/\delta q$, we express the action in terms of its Lagrangian:

$$\frac{\delta A}{\delta q_{\mathbf{k},j}} = \frac{\Delta t}{2}\left(\frac{\delta L}{\delta q_{\mathbf{k},j+\frac{1}{2}}} + \frac{\delta L}{\delta q_{\mathbf{k},j-\frac{1}{2}}}\right) - \left(\frac{\delta L}{\delta \dot{q}_{\mathbf{k},j+\frac{1}{2}}} - \frac{\delta L}{\partial \dot{q}_{\mathbf{k},j-\frac{1}{2}}}\right), \tag{46}$$

where the variations of the Lagrangian are explicitly given as

$$\frac{\delta L}{\delta \dot{q}_{\mathbf{k},j+\frac{1}{2}}} \equiv p_{\mathbf{k},j+\frac{1}{2}} = \frac{1}{\left|f_{\mathbf{k}}\right|^2}\left[\dot{q}_{\mathbf{k},j+\frac{1}{2}} + (\mathbf{v}\cdot\nabla q)_{\mathbf{k},j+\frac{1}{2}} + \alpha\omega_{\mathbf{k},j+\frac{1}{2}} + \nu k^2\omega_{\mathbf{k},j+\frac{1}{2}}\right] \tag{47}$$

and

$$\frac{\delta L}{\delta q_{\mathbf{k},j+\frac{1}{2}}} = -(\mathbf{v}\cdot\nabla p)_{\mathbf{k},j+\frac{1}{2}} + \left\{\Delta^{-1}\left[\left(\nabla q_{j+\frac{1}{2}}\times\nabla p_{j+\frac{1}{2}}\right)\cdot\mathbf{e}_z\right]\right\}_{\mathbf{k},j+\frac{1}{2}} + \alpha p_{\mathbf{k},j+\frac{1}{2}} + \nu k^2 p_{\mathbf{k},j+\frac{1}{2}}. \tag{48}$$

Notice that the expressions p, $(\mathbf{v}\cdot\nabla p)$, and $\Delta^{-1}\left[(\nabla q\times\nabla p)\cdot\mathbf{e}_z\right]$ are defined only on the staggered grid indexed by $\{j+1/2\}$. Consequently, our notation is defined as $(\mathbf{v}\cdot\nabla p)_{\mathbf{k},j+\frac{1}{2}} = (\mathbf{v}_{j+\frac{1}{2}}\cdot\nabla p_{j+\frac{1}{2}})_{\mathbf{k}}$. To evaluate these quantities back onto the original grid, we interpolate the quantities by $p_{\mathbf{k},j} = (p_{\mathbf{k},j+\frac{1}{2}} + p_{\mathbf{k},j-\frac{1}{2}})/2$.

Finally, after some straightforward mathematics, we arrive at the numerical expression for the first variation of the action function with respect to q:

$$\frac{\delta A}{\delta q_{\mathbf{k},j}} = \Delta t\left[\dot{p}_{\mathbf{k},j} - (\mathbf{v}\cdot\nabla p)_{\mathbf{k},j} + \left\{\Delta^{-1}\left[(\nabla q\times\nabla p)\cdot\mathbf{e}_z\right]\right\}_{\mathbf{k},j} + \alpha p_{\mathbf{k},j} + \nu k^2 p_{\mathbf{k},j}\right] \tag{49}$$

where the time derivative of p is the standard central finite difference expression $\dot{p}_{\mathbf{k},j} = (p_{\mathbf{k},j-\frac{1}{2}} - p_{\mathbf{k},j+\frac{1}{2}})/\Delta t$.

5. Numerical predictions for the most probable rare transitions

To show that the minimum action method is suitable for the prediction of rare transitions in turbulent models, we consider a series of examples that verifies the algorithm. In this section we begin by considering the over-damped limit of the barotropic quasi-geostrophic dynamics where the nonlinearity is assumed to be absent. We follow with an example that satisfies the equilibrium hypothesis of section 3 in a regime of a single global dynamical attractor. Through this example, we verify that the numerically obtained transition agrees with the prediction made through the equilibrium theory. Finally, we consider a geophysical-based example of considering a transition between two distinct zonal jet configurations modeled by the quasi-geostrophic equations. In all cases, we show good agreement of the numerical prediction with analytical predictions.

5.1. The over-damped limit

The over-damped limit $\alpha,\ \nu \gg 1$ of the barotropic quasi-geostrophic equations corresponds to dynamics that are dominated by dissipative effects. Therefore, we can make the assumption that the nonlinearity is subdominant and can be neglected. Moreover, for simplicity, we assume also that the topography is absent ($h = 0$). We remark that this limit, although unphysical in reality, provides a simple way of verifying the minimization procedure of the minimum action method. Absence of nonlinearity reduces the system to a linear problem, allowing for a theoretical treatment. Indeed, the instanton equation (18) become a series of linearly independent differential equations for each Fourier amplitude that can be straightforwardly solved. The over-damped dynamics are given as

$$\frac{\partial\omega}{\partial t} = -\alpha\omega - \nu(-\Delta)^n\omega + \sqrt{2\alpha\gamma}\,\eta, \tag{50a}$$

$$\mathbf{v} = \mathbf{e}_z \times \nabla\psi, \qquad \omega = \Delta\psi. \tag{50b}$$

Due to the linearity of equation (50*a*), the dynamics of the Fourier representation of the vorticity field ω can be represented as a series of uncoupled Ornstein–Uhlenbeck processes for each Fourier amplitude $\omega_{\mathbf{k}}$. This linearity means that the instanton equations can be solved directly, yielding a theoretical prediction for a rare transition between two states for a transition time T. By working in the Fourier representation, the instanton equations can be reduced to series of second-order linear boundary value problems for each Fourier amplitude:

$$\frac{\partial^2 \omega_{\mathbf{k}}}{\partial t^2} = \left(\alpha + \nu k^2\right)^n \omega_{\mathbf{k}}, \tag{51a}$$

$$\omega(\mathbf{k}, 0) = \omega_{\mathbf{k}}(0), \quad \omega(\mathbf{k}, T) = \omega_{\mathbf{k}}(T). \tag{51b}$$

Notice that the noise correlation $|f_{\mathbf{k}}|$ drops out of the instanton equations, meaning that the trajectory is independent of the noise—this is a consequence of the decoupling of each Fourier amplitude from every other. Equation (51) can be readily solved with the solution

$$\omega^\star(\mathbf{r}, t) = \sum_{\mathbf{k}} \omega^\star_{\mathbf{k}}(t)\mathbf{e}_{\mathbf{k}}(\mathbf{r}), \tag{52a}$$

with

$$\omega^\star_{\mathbf{k}}(t) = \frac{\sinh\left(\beta_{\mathbf{k}}[T-t]\right)\omega_{\mathbf{k}}(0) + \sinh\left(\beta_{\mathbf{k}}t\right)\omega_{\mathbf{k}}(T)}{\sinh\left(\beta_{\mathbf{k}}T\right)}, \tag{52b}$$

where we have used the notation $\beta_{\mathbf{k}} = \alpha + \nu k^{2n}$. As one can observe from solution (52), the most probable rare transition corresponds to an exponential decay from the initial state at a rate $\beta_{\mathbf{k}}$ followed by an exponential increase at the same rate to the final state. In essence, the transition wants to decay to the zero state, with the relaxation defined by the dissipation rate $\beta_{\mathbf{k}}$ for each Fourier mode. Once decayed, the trajectory transitions to the final state, with an exponential rate governed again by the dissipation rate. It should be noticed that for large transition times T, the majority of the transition will result in the state being close to zero, with most of the dynamics occurring at the beginning and at the end of the transition on a timescale defined by the dissipation rate $\beta_{\mathbf{k}}$. Moreover, it is worth commenting that no other alternative families of solutions exist other than the over-damped solution (52).

The corresponding Lagrangian for the theoretically predicted rare transition (52) is given by

$$\begin{aligned}\mathcal{L}\left[\omega^\star, \frac{\partial\omega^\star}{\partial t}\right] &= \frac{1}{2}\int_D \int_D \left[\frac{\partial\omega^\star}{\partial t} + \alpha\omega^\star + \nu(-\Delta)^n\omega^\star\right](\mathbf{r}) \\ &\quad \times C^{-1}(\mathbf{r}, \mathbf{r}')\left[\frac{\partial\omega^\star}{\partial t} + \alpha\omega^\star + \nu(-\Delta)^n\omega^\star\right](\mathbf{r}')\, \mathrm{d}\mathbf{r}\, \mathrm{d}\mathbf{r}' \\ &= \frac{1}{2}\sum_{\mathbf{k}} \frac{\beta_{\mathbf{k}}\exp\left(2\beta_{\mathbf{k}}t\right)}{|f_{\mathbf{k}}|^2\sinh^2\left(\beta_{\mathbf{k}}T\right)}\left|\omega_{\mathbf{k}}(T) - \omega_{\mathbf{k}}(0)\exp\left(\beta_{\mathbf{k}}T\right)\right|^2.\end{aligned} \tag{53}$$

The Lagrangian (53) quantifies how much momentum is required from the noise to push the transition to the final state. Therefore, it is an important quantity for the rare transition, characterizing the effect of the noise along the transition, and also yields the action upon time integration.

We now test the minimum action method and compare the numerically obtained transition path with that predicted by the theory. We apply the numerical method to the over-damped system previously defined. We select the initial and final states to be $\omega_0 = [\cos(x) - (2/5)\sin(x) + (1/5)\cos(y) + (3/5)\cos(x+y) - (4/5)\sin(2y-x)]/E$ and $\omega_T = [(1/2)\cos(x) + (2/5)\sin(x) + (3/5)\cos(3y) - (1/5)\cos(2y-x) + (1/5)\sin(2y-x)]/E$, appropriately normalized through E to give unit energy density. The two states are displayed in figure 6 and were chosen so that they contain a large number of modes. We perform the minimization with an initial trajectory defined through linear interpolation between the two boundary states in time. We use $N_x = N_y = 16$ Fourier modes and a temporal grid of $N_t = 100$ points for a periodic spatial domain of size $L_x = L_y = 2\pi$ and a time domain of length $T = 10$. The dissipation parameters that we use are $\alpha = 1 \times 10^{-1}$ and $\nu = 5 \times 10^{-2}$, with $n = 1$. We choose a noise correlation that represents a Gaussian white noise with $C(\mathbf{r} - \mathbf{r}') = \delta(\mathbf{r} - \mathbf{r}')/Z$, where Z is the normalization constant to ensure relation (6) holds.

Displayed in figure 7 (left) is the time evolution of absolute value of each Fourier mode in the transition and (right) the complex phase space of the transition of each Fourier mode. In both plots, the theoretical predictions arising from equation (52) are overlaid by the dashed black curves. We observe excellent agreement between the

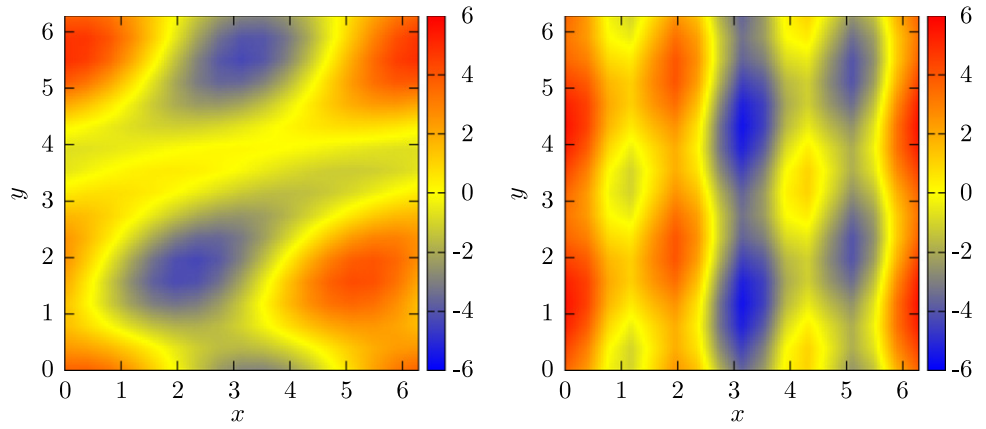

Figure 6. We plot the vorticity distribution of the initial $\omega_0 = [\cos(x) - (2/5)\sin(x) + (1/5)\cos(y) + (3/5)\cos(x+y) - (4/5)\sin(2y-x)]/E$ and final $\omega_T = [(1/2)\cos(x) + (2/5)\sin(x) + (3/5)\cos(3y) - (1/5)\cos(2y-x) + (1/5)\sin(2y-x)]/E$ states, appropriately normalized through the constant E to give unit energy density.

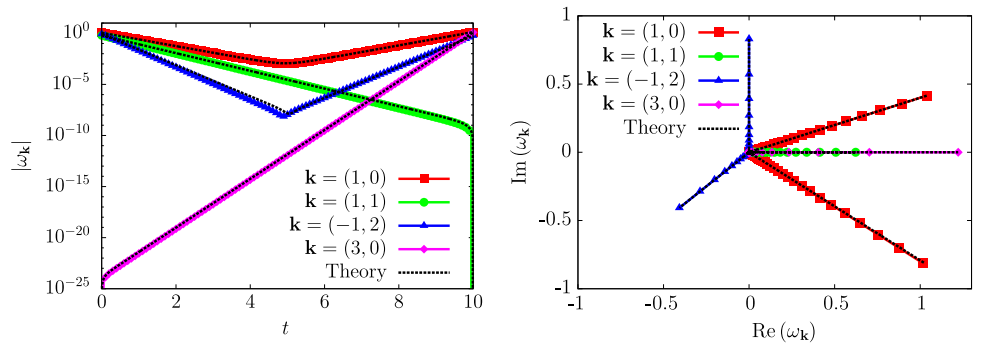

Figure 7. (Left) We plot the time evolution of $|\omega_{\mathbf{k}}(t)|$ for each mode $\mathbf{k}$. (Right) We plot the complex phase space trajectories of each mode. For each, the theoretical prediction of equation (52) is overlaid by a dashed black curve.

numerical and theoretical results. We observe a slight discrepancy with the numerical data in the time evolution of mode $\mathbf{k} = (-1, 2)$, but this is certainly due to numerical resolution close to the cusp, where the transition goes from exponential decay to growth near $t = 5$. In figure 7 (right), we quite clearly observe that the transition quickly decays to the zero state for each Fourier amplitude before transitioning to the final state. In figure 8 we plot the time evolution of the Lagrangian for the numerical prediction and compare with the theoretical result given by (53). We observe excellent agreement with the theory and see that the majority of the Lagrangian appears at later times where the transition needs to be pushed against the dissipation to reach the final state.

We conclude that the numerical minimization for the over-damped system yields the expected results predicted through the Freidlin–Wentzell theory. However, we stress that this example ignores the effect of the nonlinear advection term of the quasi-geostrophic equations, which we discuss in the next subsections.

5.2. Equilibrium instanton starting at zero

In this subsection, we consider applying the minimum action method to an example that satisfies the equilibrium hypothesis of section 3. Such an example will allow for the direct comparison with the predictions made in section 3, thus verifying not only the numerical optimization algorithm but also the equilibrium theory. Our setup will be the following: we will consider a transition beginning at the zero state and transitioning to another, nonzero, state. What is essential is that we compute this transition in the equilibrium regime where there is only one global dynamical attractor, the zero state. This is important because we want to compare the numerical prediction with the solution defined through relaxation from the time-reversed transition in the corresponding dual dynamics defined through the relaxation equation (23). The criterion of zero being the only attractor is important because this comparison can be made only if the transition remains in the same basin of attraction as that of the attractor in which the transition starts. (Transitions that occur across several basins of attraction will have to be compared with a theoretical transition composed of several instantons and relaxation trajectories corresponding to each attractor and saddle that the transition passes through.) By considering a

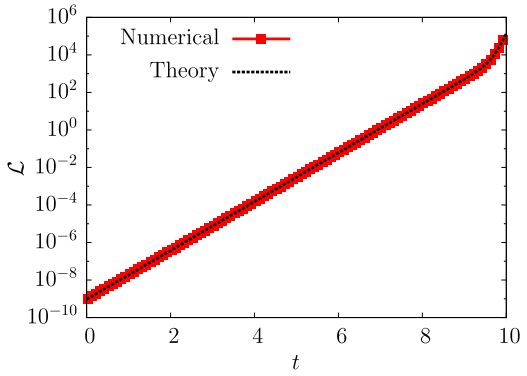

Figure 8. Time evolution of the Lagrangian $\mathcal{L}$ for the over-damped problem. The theoretical result of (53) is plotted by the dashed black curve.

setup with only one attractor, all possible nonzero states will be within the basin of attraction $\omega = 0$ and the transition can be compared with one instanton prediction through the relaxation equations.

In general, determining a transition from zero to an arbitrary state ω_T analytically is difficult. However, ensuring the equilibrium hypothesis holds will help us in this regard. We know from section 3 that the rare transition from an attractor to any state within the basin of attraction of that attractor will be the time-reversed relaxation path of the corresponding dual system. Therefore, by considering the relaxation path equation (23), we will recover the instanton: the most probable infinite time fluctuation path. Unfortunately, due to the numerical discretization of the minimum action method, we are unable to ascertain the infinite time transition path. However, one would expect that if T is sufficiently large, the two transitions should be relatively close. Therefore, we will consider a sequence of transitions for increasing T and show convergence to the instanton.

The equilibrium setup is as follows: we consider a noise spectrum that is uniform in Fourier space, i.e., corresponding to a Gaussian white noise with a correlation $C(\mathbf{r}, \mathbf{r}') = \delta(\mathbf{r} - \mathbf{r}')/Z$ and a potential that is proportional to the enstrophy measure $\mathcal{G} \propto \omega^2/2$. This is important for three reasons: *i)* this corresponds to linear friction in the two-dimensional Euler equations, meaning that the model is realistic in some sense; *ii)* this potential and the noise correlation satisfy the equilibrium hypothesis of section 3; and *iii)* the quadratic form of the potential implies that only one minimum corresponds in this case to the zero state $\omega = 0$.

For the numerics, we choose the final state to be $\omega_T = [\cos(x) - (2/5)\sin(x) + (2/5)\cos(x + y) - (1/2)\sin(x + y) + (3/5)\cos(2x + y) - (1/5)\sin(2x + y)]/E$, where E is the normalization constant to give unit energy density.

We use a Fourier resolution of $N_x = N_y = 16$ Fourier harmonics in the minimum action method and compare a series of minimizations with increasing transition time T. In each realization we ensure that we have sufficient temporal resolution by using a fixed grid spacing of $T/N_t = 10^{-1}$.

In figure 9 we show the vorticity distribution of the final transition state (left) and the time evolution of the transition energy $\mathcal{E}$ (right). Notice that from the energy balance equation (9), we expect an exponential decrease of the energy at the rate 2α. This is exactly what is observed from the relaxation trajectory (dashed black line in figure 9). Moreover, observe that the numerical minimization predictions also agree with this decay rate initially. The discrepancy at later times is a consequence of the minimization procedure dealing only with a transition of finite transition time T, such that the energy must vanish in finite time. This is also supported by the observation that increasingly longer transition times result in better agreement with the expected energy decay. Of course, one expects, and this is indicated by the numerics, that this agreement will be exact in the limit of $T \to \infty$.

We plot the complex phase space trajectories for each Fourier mode in figure 10. Again, we observe gradual convergence to the theoretical infinite transition time prediction computed through the relaxation equation. Notice the complex behavior of the transition associated with the nonlinear nature of the evolution. Finally, in figure 11 we plot the instanton Hamiltonian for the numerical minimum action predictions for the various transition times T. We observe fairly good stationarity of the Hamiltonian across the time evolution for transition times T. Notice that the value of the Hamiltonian decreases with increasing transition time T. We expect that the value of the instanton Hamiltonian should decrease with increasing transition time T.

Through this example, we have verified that the numerical predictions for the most probable rare transition from zero to an arbitrary state using the minimum action method agree with the theoretical prediction made using the equilibrium hypothesis of section 3. Through this, we have also independently confirmed that the predictions of rare transitions in equilibrium cases can be verified through the relaxation dynamics of a corresponding dual system.

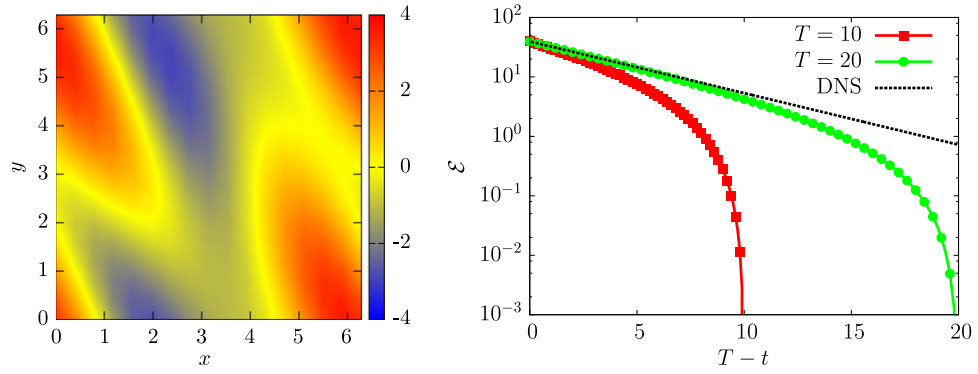

Figure 9. (Left) The final transition state $\omega_T = [\cos(x) - (2/5)\sin(x) + (2/5)\cos(x+y) - (1/2)\sin(x+y) + (3/5)\cos(2x+y) - (1/5)\sin(2x+y)]/E$, where E is a normalization constant to give unit energy density. (Right) The time evolution of energy of the predicted transition path for transition times $T = 10$ and $T = 20$ compared with the relaxation trajectory from direct numerical simulation corresponding to the $T \to \infty$ limit.

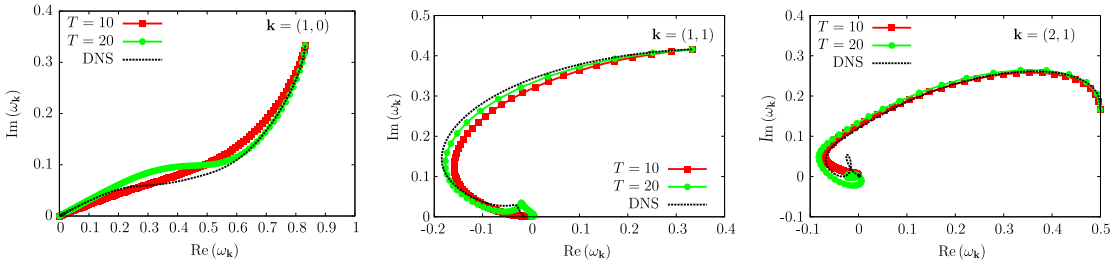

Figure 10. Complex phase space trajectories of each of the Fourier modes of the final state for $\mathbf{k} = (1, 0)$ (left), $\mathbf{k} = (1, 1)$ (middle), $\mathbf{k} = (2, 1)$ (right) for transition times $T = 10$ and $T = 20$. The dashed black curve corresponds to the $T \to \infty$ limit computed using the relaxation equation (23).

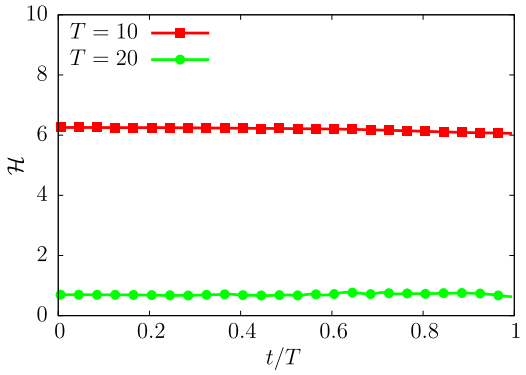

Figure 11. Plot of the instanton Hamiltonian for the numerical minimization predictions from the minimum action method for transition times $T = 10$ and $T = 20$.

5.3. A non-equilibrium geophysical example: Action minimization between two zonal flow states

In this subsection we consider a more general example which is of huge interest to the geophysical community—namely, an action minimizer between two zonal jet configurations for the barotropic quasi-geostrophic equations with topography and forced by statistically homogeneous noise. This example does not verify the equilibrium hypothesis of section 3.

The importance of this example is based on its practicality. A transition between two zonal flow states is something that arises in nature, for instance in ocean currents and atmospheric dynamics. Moreover, the existence of multiple zonal jet attractors in geophysical models has also recently been observed [36], meaning that a transition between them in the presence of stochastic fluctuations is an important and viable problem.

Mathematically, the problem is an intriguing one because the set of all zonal states in the periodic barotropic quasi-geostrophic equations ($q(\mathbf{r},\,t) \equiv q(y,\,t)$) forms a vector space of steady-state solutions of the dynamics where the condition $\mathbf{v}\cdot\nabla q = 0$ is always satisfied. By considering the transition between two zonal flow states, there always exists a critical point of the action (a solution to the Euler–Lagrange equations) that remains in the vector space of zonal flows as long as the noise is non-degenerate in the zonal direction. The noise is non-degenerate if the spatial correlation defines a symmetric operator that is definite-positive. For a spatially homogeneous correlation function, this definition is equivalent to the property that all Fourier coefficients of the spatial correlation function (the spatial noise correlation spectrum) are strictly positive. As discussed hereafter, this zonal critical point of the action verifies simple equations, enabling us to make analytical predictions. We stress, however, that it is not granted that this zonal critical point is an action minimizer or even a local action minimizer. In this section, for a specific example, we will use the action minimization algorithm to check that this critical point of the action is actually a local minimizer.

First, let us begin by investigating the theoretical problem. Consider the path between two generic zonal flows (without loss of generality, we assume the zonal direction to be x), e.g., $q(\mathbf{r},\,0) = q_0(y)$ and $q(\mathbf{r},\,T) = q_T(y)$, with topography varying only across y: $h(\mathbf{r}) = h(y)$. As mentioned previously, we study the action minimizer between two zonal flows that occur through other zonal states. Subsequently, the equations for the minimizer are:

$$q^\star(y,\,t) = \gamma(t)\Big[q_T(y) - q_0(y)\Big] + q_0(y), \tag{54a}$$

$$\gamma(0) = 0, \quad \gamma(T) = 1. \tag{54b}$$

To find the structure of the parameterized path $\gamma(t)$, we insert an ansatz (54) into the instanton equation (18). Due to the ansatz requiring the minimizer to remain through zonal steady states, all nonlinear terms identically vanish in the instanton equations. Then these Euler–Lagrange equations simplify to

$$\frac{\partial^2\omega^\star(y,\,t)}{\partial t^2} = \left[\alpha + \nu\left(-\frac{\partial^2}{\partial y^2}\right)^n\right]^2\omega^\star(y,\,t), \tag{55a}$$

$$\omega(y,\,0) = q_0(y) - h(y), \quad \omega(y,\,T) = q_T(y) - h(y), \tag{55b}$$

where $\omega^\star(t) = \gamma(t)\Big[q_T(y) - q_0(y)\Big] + q_0(y) - h(y)$. The reason for expressing (55) in terms of the vorticity ω and not the potential vorticity q is that the topography h appears only in the definition of the boundary states and not in the equation of motion itself. We can then straightforwardly solve (55) for each Fourier amplitude because the system is linear in ω. Subsequently, writing the solution in terms of the Fourier amplitudes for ω is more transparent:

$$\omega^\star(y,\,t) = \sum_{k_y}\omega^\star_{k_y}(t)\,\mathbf{e}_{k_y}(y), \tag{56a}$$

with

$$\omega^\star_{k_y}(t) = \frac{1}{\sinh\left(\beta_{k_y}T\right)}\left[\sinh\Big(\beta_{k_y}\left[T-t\right]\Big)\omega_{k_y}(0) + \sinh\Big(\beta_{k_y}t\Big)\omega_{k_y}(T)\right], \tag{56b}$$

where $\mathbf{e}_{k_y} = \exp\Big(ik_y y\Big)\Big/L_y^{1/2}$. We have represented the action minimizer in terms of $\omega^\star_{k_y}(t) = q^\star_{k_y}(t) - h_{k_y}$, where h_{k_y} are Fourier coefficients of the topography $h(y) = \sum_{k_y} h_{k_y}\mathbf{e}_{k_y}$ and $\beta_{k_y} = \alpha + \nu k_y^{2n}$. Solution (56) can be transformed back into the solution for the potential vorticity using $q^\star_{k_y}(t) = \omega^\star_{k_y}(t) - h_{k_y}$. What should be noticed is that the transition (56) is reminiscent of the over-damped solution presented in subsection 5.1. This is because the zonal–zonal minimizer path occurs through the vector space of zonal flows and the nonlinearity vanishes throughout the transition. Therefore, one can think of the zonal–zonal action minimizer as the same as the over-damped solution or in terms of an Ornstein–Uhlenbeck process with the transition exponentially diffusing across steady states. What is also interesting is that the solution does not depend on the type of topography as long as it is defined along y only.

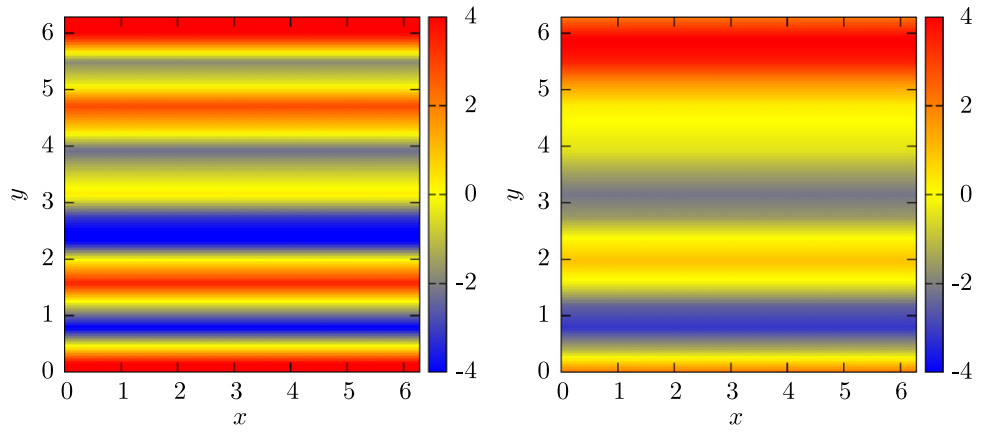

Figure 12. The vorticity distribution of the initial and final zonal flow states: $\omega_0 = [\cos(y) - (2/5)\sin(y) + (4/5)\cos(3y) - (3/5)\sin(3y) + 2\cos(4y)]/E$ and $\omega_T = [\cos(y) - \sin(y) - (3/2)\sin(2y) + (4/5)\cos(3y) - (4/5)\sin(3y)]/E$, with E being the normalization constant to ensure unit energy density in each case.

The explicit expression for the Lagrangian for trajectory (56) is given by

$$\mathcal{L}\left[q^\star, \frac{\partial q^\star}{\partial t}\right] = \frac{1}{2}\int_D \int_D \left[\frac{\partial q^\star}{\partial t} + \alpha\omega^\star + \nu\left(-\frac{\partial^2}{\partial y}\right)^n \omega^\star\right](y) \times C_z^{-1}(y-y')\left[\frac{\partial q^\star}{\partial t} + \alpha\omega^\star + \nu\left(-\frac{\partial^2}{\partial y'}\right)^n \omega^\star\right](y')\,\mathrm{d}y\,\mathrm{d}y' = \frac{1}{2}\sum_{k_y} \frac{\beta_{k_y}\exp\left(2\beta_{k_y}t\right)}{\left|f_{k_y}\right|^2 \sinh^2\left(\beta_{k_y}T\right)}\left|\omega_{k_y}(T) - \omega_{k_y}(0)\exp\left(\beta_{k_y}T\right)\right|^2, \tag{57}$$

where C_z is the zonal part of the noise correlation function defined by (34).

To perform the numerical minimization, we select two zonal flow states given by $\omega_0 = [\cos(y) - (2/5)\sin(y) + (4/5)\cos(3y) - (3/5)\sin(3y) + 2\cos(4y)]/E$ and $\omega_T = [\cos(y) - \sin(y) - (3/2)\sin(2y) + (4/5)\cos(3y) - (4/5)\sin(3y)]/E$, where E is the appropriate normalization constant. Both these states are displayed in figure 12. We use a linear friction coefficient of $\alpha = 1 \times 10^{-1}$ and normal viscosity ($n = 1$) with coefficient $\nu = 5 \times 10^{-2}$. We consider a transition occurring over a time of $T = 10$ with a temporal resolution of $N_t = 200$ grid points. Our Fourier resolution is $N_x = N_y = 16$ on a periodic square domain of size $L_x = L_y = 2\pi$. For the noise, our only conditions are that it be homogeneous and non-degenerate. Therefore, we choose a noise spectrum of the form

$$f_{\mathbf{k}} = \frac{1}{Z}\frac{k^2}{k_f^2}\exp\left(-\frac{k^2}{k_f^2}\right)\exp\left(i\frac{\pi}{4}\right), \tag{58}$$

with $k_f = 3$ and Z being the normalization constant to ensure condition (6) is satisfied. The profile of the forcing is shown in figure 13. As one can observe, the noise is isotropic and peaks at wavenumber $k = 3$, with a Gaussian profile around this peak.

In figure 14 we plot the time evolution of the action minimizer from the initial to the final state in terms of a Hovmöller diagram. A more illustrative comparison with the theory can viewed in figure 15, which shows the time evolution of the zonal Fourier amplitudes of the numerically predicted minimizer (left) and also the evolution of each mode in the complex phase space (right). Overlaid in both of the plots with dashed black curves is the theoretically predicted action minimizer from equation (56). We observe excellent agreement between the numerical data and theory, indicating that the minimum action method has located a local action minimizer of the action that coincides with the theoretical zonal critical point.

As additional checks, we present the time evolution of the Lagrangian (57) and instanton Hamiltonian (17) in figure 16, with the theoretical predictions overlaid in black. Again, we observe that the theory agrees with the numerical data. The Lagrangian indicates that most of the effort is in pushing the trajectory to the final state near the end of the evolution. The constant value of the Hamiltonian throughout the path is another indicator that the minimum action method has found a local minimum.

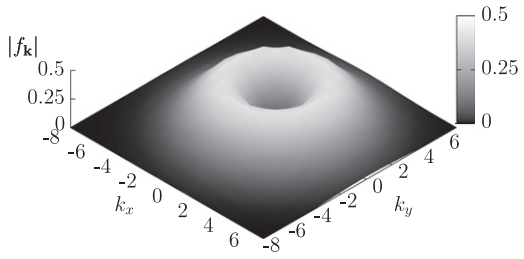

Figure 13. Spectral distribution of the noise spectrum $|f_{\mathbf{k}}|$, normalized by condition (6).

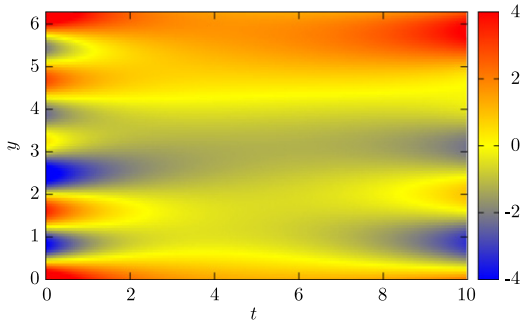

Figure 14. Hovmöller diagram of the zonal flow action minimizer.

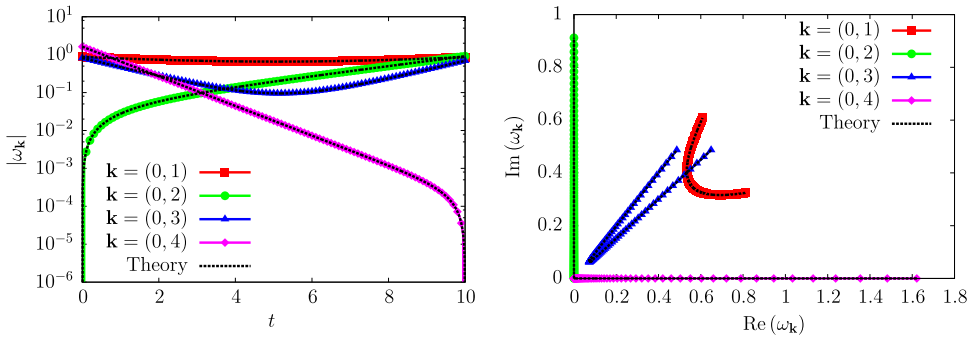

Figure 15. (Left) Time evolution of the modulus of zonal Fourier harmonics of modes $\mathbf{k} = (0, 1), \mathbf{k} = (0, 2), \mathbf{k} = (0, 3)$, and $\mathbf{k} = (0, 4)$. The dashed black curve overlays the theoretical prediction from (56). (Right) The phase space trajectories of the zonal Fourier harmonics from the numerically found action minimizer and the prediction of (56).

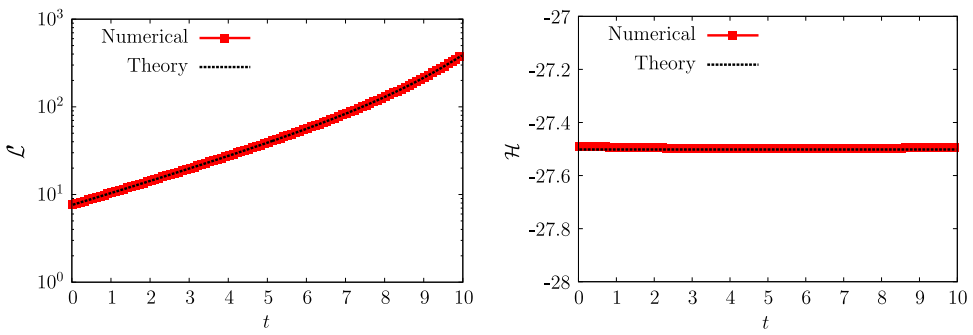

Figure 16. (Left) Evolution of the Lagrangian (57) with comparison with the theoretical prediction. (Right) Time evolution of the instanton Hamiltonian (17) with comparison with the theoretical value obtained from (56).

As can be observed from the expression of the Lagrangian for this setup (57), the amplitude of the noise plays an essential role in determining which Fourier modes contribute to the Lagrangian and hence the action. An important remark in this example is that the noise correlation will not have a direct effect on the shape of the action minimizer, this being due to the nonlinear terms vanishing, but will be essential for determining the specific value of the action corresponding to the minimizer.

The preceding example illustrates the local stability of an action minimizer between two zonal flows. We predict that the trajectory of the minimizer will remain through the vector space of zonal flows, with the structure of the transition being independent of the non-degenerate noise correlation. Because the action minimizer remains through connected steady states, we do not know at this point whether the Freidlin–Wentzell theory is valid or whether the action minimizer corresponds to a rare transition. However, this is a first step toward understanding (in a numerical context) rare transitions observed in direct numerical simulations of the quasi-geostrophic equations in regimes like the ones in [36], where multiple zonal jets have been observed as dynamical attractors.

The preceding result for the action minimizer between two zonal flow states can be generalized in the context of an action minimizer between two steady states that are formed from eigenfunctions of the Laplacian operator Δ with the same eigenvalue λ, where $-\Delta q = \lambda q$. This is because the set of states constructed by eigenfunctions of the Laplacian also form a vector space of steady-state solutions with $\mathbf{v} \cdot \nabla q = 0$. Consequently, if both states, initial and final, are constructed with the same sets of eigenfunctions with identical eigenvalues, then we expect a result similar to the foregoing.

6. Conclusions

We have adapted a numerical optimization algorithm called the minimum action method and applied it to a simple model of two-dimensional geophysical turbulence. We have shown, using specific examples, that such an algorithm can be used to compute the most probable rare transitions between two states in cases of bistability in turbulent systems. Using the equilibrium theory derived in [28], we showed how the numerically predicted transition agreed with those computed through the relaxation equations of the corresponding dual system when the equilibrium hypothesis holds. Furthermore, we considered a more general problem of computing the most probable transition between two different zonal flow configurations where the equilibrium hypothesis does not hold—an important example of relevance to geophysics.

The minimum action method is a viable way to compute rare events in simple turbulent models. It is straightforward to extend this method to more complex turbulent models such as magneto-hydrodynamics, where rare transitions between different magnetic field polarizations can be observed [14]. Moreover, natural extensions to the algorithm proposed here could be of benefit, such as arc length parameterization of time [69], adaptive discretization [64], and parallelization [67].

Clearly, the next step in this approach is to compare the action minimizers with observed transitions in both experiments and direct numerical simulations. Indeed, this is one of the current directions of future work. Besides this direct comparison, much work is still to be done both at the theoretical and at the practical level in order to actually assess when minimum action methods alone will be enough to describe rare transitions. This is certainly true when we are in a Freidlin–Wentzell regime, as discussed in subsection 2.2; however, for most turbulence models no clear criteria have yet been developed to assess when a rare transition in a turbulent flow is actually in the Freidlin–Wentzell regime. This is an important question that should be addressed from both a theoretical and an empirical point of view.

This work is a step in a long-term program that is aimed at developing the tools to compute rare transitions and their probabilities in complex turbulent flows. Our ultimate aim is to be able to make these computations for models that are relevant to climate dynamics. Of course, much is still to be achieved in this direction before climate applications can truly be considered. However, it is important to stress that no approach currently makes it possible to reliably compute rare transition in climate problems.

Acknowledgments

The research leading to these results has received funding from the European Research Council under the European Union's Seventh Framework Programme (FP7/2007–2013 Grant Agreement no. 616811) (F. Bouchet). The research has also been supported through the ANR program STATOCEAN (ANR-09-SYSC-014) (J. Laurie) and the PSMN (Pôle Scientifique de Modélisation Numérique) computing center of ENS de Lyon.

References

[1] Benzi R 2005 *Phys. Rev. Lett.* **95** 024502
[2] Rahmstorf S 2002 *Nature* **419** 207–14
[3] Ganopolski A and Rahmstorf S 2002 *Phys. Rev. Lett.* **88** 038501
[4] Schmeits M J and Dijkstra H A 2001 *J. Phys. Oceanogr.* **31** 3435–56
[5] Qiu B and Miao W 2000 *J. Phys. Oceanogr.* **30** 2124–37
[6] Charney J G and DeVore J G 1979 *J. Atmos. Sci.* **36** 1205–16
[7] Kravtsov S, Robertson A W and Ghil M 2005 *J. Atmos. Sci.* **62** 1746–69
[8] Farrell B F and Ioannou P J 2003 *J. Atmos. Sci.* **60** 2101–18
[9] Saravanan R 1993 *J. Atmos. Sci.* **50** 1211–27
[10] Chen G, Held I M and Robinson W A 2007 *J. Atmos. Sci.* **64** 2899–915
[11] Weeks E R, Tian Y, Urbach J S, Ide K, Swinney H L and Ghil M 1997 *Science* **278** 1598–601
[12] Chavaillaz Y, Codron F and Kageyama M 2012 *Clim. Past Discuss.* **8** 3693–717
[13] Toggweiler J R, Russell J L and Carson S R 2006 *Paleoceanography* **21** PA2005
[14] Berhanu M 2007 *Europhys. Lett.* **77** 59001
[15] Sommeria J 1986 *J. Fluid Mech.* **170** 139–68
[16] Maassen S R, Clercx H J H and van Heijst G J F 2003 *J. Fluid Mech.* **495** 19–33
[17] Bouchet F and Simonnet E 2009 *Phys. Rev. Lett.* **102** 094504
[18] Chandra M and Verma M K 2011 *Phys. Rev.* E **83** 067303
[19] Niemela J J, Skrbek L, Sreenivasan K R and Donnelly R J 2001 *J. Fluid Mech.* **449** 169–78
[20] Sugiyama K, Ni R, Stevens R J A M, Chan T S, Zhou S Q, Xi H D, Sun C, Grossmann S, Xia K Q and Lohse D 2010 *Phys. Rev. Lett.* **105** 034503
[21] Brown E and Ahlers G 2006 *J. Fluid Mech.* **568** 351–86
[22] Ravelet F, Marié L, Chiffaudel A and Daviaud F 2004 *Phys. Rev. Lett.* **93** 164501
[23] Benzi R, Parisi G, Sutera A and Vulpiani A 1982 *Tellus* **34** 10–16
[24] Benzi R, Sutera A and Vulpiani A 1981 *J. Phys. A: Math. Gen.* **14** L453
[25] Hays J D, Imbrie J and Shackleton N J 1976 *Science* **194** 1121–32
[26] Ghil M 1994 *Physica* D **77** 130–59
[27] Pétrélis F and Fauve S 2010 *Phil. Trans. R. Soc.* A **368** 1595–605
[28] Bouchet F, Laurie J and Zaboronski O 2014 *J. Stat. Phys.* **156** 1066–92
[29] Zinn-Justin J 2002 *Quantum Field Theory and Critical Phenomena* (Oxford: Clarendon Press) ISBN 9780198509233
[30] Freidlin M I and Wentzell A D 1984 *Random Perturbations of Dynamical Systems* (New York, Berlin: Springer)
[31] Faris W G and Jona-Lasinio G 1982 *J. Phys. A: Math. Gen.* **15** 3025
[32] Jona-Lasinio G and Mitter P K 1985 *Commun. Math. Phys.* **101** 409–36
[33] Hairer M, Maas J and Weber H 2014 *Comm. Pure Appl. Math.* **67** 776–870
[34] Hairer M and Weber H 2014 arXiv:1404.5863 [math-ph]
[35] Bouchet F and Venaille A 2012 *Phys. Rep.* **515** 227–95
[36] Constantinou N C, Farrell B F and Ioannou P J 2014 *J. Atmos. Sci.* **71** 1818–42
[37] Pedlosky J 1987 *Geophysical Fluid Dynamics* (New York: Springer) ISBN 978–0-387–96387-7
[38] Fjørtoft R 1953 *Tellus* **5** 225–30
[39] Salmon R, Holloway G and Hendershott M C 1976 *J. Fluid Mech.* **75** 691–703
[40] Bretherton F P and Haidvogel D B 1976 *J. Fluid Mech.* **78** 129–54
[41] Miller J 1990 *Phys. Rev. Lett.* **65** 2137–40
[42] Robert R and Sommeria J 1991 *J. Fluid Mech.* **229** 291–310
[43] Feynman R P and Hibbs A R 1965 *Quantum mechanics and path integrals* (New York: McGraw-Hill)
[44] Wio H S, Colet P, San M M, Pesquera L and Rodríguez M A 1989 *Phys. Rev.* A **40** 7312–24
[45] Onsager L and Machlup S 1953 *Phys. Rev.* **91** 1505–12
[46] Machlup S and Onsager L 1953 *Phys. Rev.* **91** 1512–5
[47] Grafke T, Grauer R, Kumar T and Vanden-Eijnden E 2014 *Multiscale Model. Simul.* **12** 566–80
[48] Kraichnan R H and Montgomery D 1980 *Rep. Prog. Phys.* **43** 547–619
[49] Bouchet F and Corvellec M 2010 *J. Stat. Mech.* **2010** P08021
[50] Bouchet F 2008 *Physica* D **237** 1976–81
[51] Chavanis P H 2003 *Phys. Rev.* E **68** 036108
[52] Chavanis P H 2009 *Eur. Phys. J.* B **70** 73–105
[53] Corvellec M and Bouchet F 2012 arXiv:1207.1966 [cond-mat, physics:physics]
[54] Chavanis P H and Sommeria J 1996 *J. Fluid Mech.* **314** 267–97
[55] Venaille A and Bouchet F 2009 *Phys. Rev. Lett.* **102** 104501
[56] Gottlieb D and Orszag S A 1977 *Numerical Analysis of Spectral Methods:Theory and Applications* (Philadelphia: Society for Industrial and Applied Mathematics) ISBN 9780898710236
[57] E W, Ren W and Vanden-Eijnden E 2002 *Phys. Rev.* B **66** 052301
[58] Ren E W and Vanden-Eijnden E W 2007 *J. Chem. Phys.* **126** 164103
[59] Jónsson H, Mills G and Jacobsen K W 1998 *Nudged elastic band method for finding minimum energy paths of transitions Classical and Quantum Dynamics in Condensed Phase Simulation* (Singapore: World Scientific) pp pp 385–404
[60] Cerjan C J and Miller W H 1981 *J. Chem. Phys.* **75** 2800–6
[61] Henkelman G and Jónsson H 1999 *J. Chem. Phys.* **111** 7010–22
[62] Grafke T, Grauer R and Schäfer T 2013 *J. Phys. A: Math. Theor.* **46** 062002
[63] E W, Ren W and Vanden-Eijnden E 2004 *Comm. Pure Appl. Math.* **57** 637–56
[64] Zhou X, Ren W and E W 2008 *J. Chem. Phys.* **128** 104111
[65] Wan X, Zhou X and E W 2010 *Nonlinearity* **23** 475–93
[66] Fogedby H C and Ren W 2009 *Phys. Rev.* E **80** 041116
[67] Wan X 2011 *J. Comp. Phys.* **230** 8669–82
[68] Heymann M and Vanden-Eijnden E 2008 *Comm. Pure Appl. Math.* **61** 1052–117

[69] Vanden-Eijnden E and Heymann M 2008 *J. Chem. Phys.* **128** 061103
[70] Nocedal J and Wright S J 2006 Numerical Optimization *Springer Series in Operations Research and Financial Engineering* 2nd edn (Berlin: Springer)